

Bose–Einstein condensation of alpha clusters and new soft mode in ^{12}C – ^{52}Fe $4N$ nuclei in field theoretical superfluid cluster model

R. Katsuragi,¹ Y. Kazama,¹ J. Takahashi,^{1,*} Y. Nakamura,^{1,2} Y. Yamanaka,^{1,†} and S. Ohkubo^{3,‡}

¹*Department of Electronic and Physical Systems, Waseda University, Tokyo 169-8555, Japan*

²*Nagano Prefectural Kiso Seiho High School, Nagano 397-8571, Japan*

³*Research Center for Nuclear Physics, Osaka University, Ibaraki, Osaka 567-0047, Japan*

(Dated: March 16, 2022)

Bose–Einstein condensation of α clusters in light and medium-heavy nuclei is studied in the frame of the field theoretical superfluid cluster model. The order parameter of the phase transition from the Wigner phase to the Nambu–Goldstone phase is a superfluid amplitude, square of the moduli of which is the superfluid density distribution. The zero mode operators due to the spontaneous symmetry breaking of the global phase in the *finite* number of α clusters are rigorously treated. The theory is systematically applied to $N\alpha$ nuclei from ^{12}C – ^{52}Fe at various condensation rates. In ^{12}C it is found that the energy levels of the gas-like well-developed α cluster states above the Hoyle state are reproduced well in agreement with experiment for realistic condensation rates of α clusters. The electric E2 and E0 transitions are calculated and found to be sensitive to the condensation rates. The profound *raison d'être* of the α cluster gas-like states above the Hoyle state, whose structure has been interpreted geometrically in the nuclear models without the order parameter such as the cluster models or *ab initio* calculations, is revealed. It is found that in addition to the Bogoliubov–de Gennes vibrational mode states collective states of the zero mode operators appear systematically at low excitation energies from the $N\alpha$ threshold energy. These collective states, new-type soft modes in nuclei due to the Bose–Einstein condensation of the α clusters, emerge systematically in light and medium-heavy mass regions and are also located at high excitation energies from the ground state in contrast to the traditional concept of soft mode in the low excitation energy region.

PACS numbers: 21.60.Gx,27.20.+n,67.85.De,03.75.Kk

I. INTRODUCTION

The nucleus shows various aspects of collective motion such as quadrupole vibration in spherical nuclei and rotation in deformed nuclei, and pairing vibration in normal nuclei and rotation in superfluid nuclei. These collective motion and the phase transitions from spherical to deformed and from normal to superfluid [1, 2] are observed in medium-heavy and heavy mass region where mean field picture works well. The emergence of quadrupole deformation and the superfluidity has been understood as a consequence of condensation of a quadrupole boson with an angular momentum $J = 2$ and a Cooper pair boson with $J = 0$, respectively. The phase transition from the Wigner phase to the Nambu–Goldstone (NG) phase in nuclei composed of *finite* number of nucleons can be understood by the order parameter, the deformation δ for the quadrupole collective motion and the pairing gap energy Δ for the pairing collective motion.

In light nuclei, collective motion due to the emergence of cluster structure, especially α cluster structure, has been studied extensively in the last decades [3–6]. The cluster model has been established as one of the three nuclear models [3–6] as well as the shell model [7, 8] and the collective model [9]. This collective motion caused by

the spontaneous symmetry breaking of rotational invariance due to the α clustering has been observed in a wide range of nuclei throughout the periodic table. Typically, they are, for example, the α + α cluster structure in ^8Be in the p-shell region [3], the α + ^{12}C structure in ^{16}O and α + ^{16}O structure in ^{20}Ne around the beginning of the sd-shell region [4], and the α + ^{36}Ar cluster structure in ^{40}Ca and the α + ^{40}Ca cluster structure in ^{44}Ti around the beginning of the fp-shell region [10–12], and the α + ^{208}Pb cluster band in ^{212}Po [13–16] in the heavy mass region.

The collective motion related to α cluster condensation or superfluidity in nuclei has been paid attention in the frame of the many-body theory in the last decades [17–19]. However, in heavy and medium-heavy mass region, α cluster superfluidity with a characteristic collective motion has not been confirmed experimentally. On the other hand, in light nuclei the Hoyle state in ^{12}C with a well-developed three α cluster structure near the α threshold energy has been extensively studied theoretically [20–29], and experimentally [30–34], and attracted much attention as a candidate for a Bose–Einstein condensation (BEC) of α clusters.

Matsumura and Suzuki [25] have shown in the cluster model calculations that the occupation probability of the α clusters sitting in the lowest 0s state is about 70% for the Hoyle state. However, from this occupation probability, whatever the 0s state occupation probability may be, it is impossible to know that the global phase of the system is frozen, that is, to conclude that the BEC of α clusters is realized. It is because the *order parameter* is

* takahashi.j@aoni.waseda.jp

† yamanaka@waseda.jp

‡ shigeo.ohkubo@rcnp.osaka-u.ac.jp

not defined in the traditional cluster models such as the generator coordinate method [21], the resonating group method [22], the cluster gas model [23, 24], the correlated Gaussian stochastic variation method [25], the orthogonality condition model [26, 27], the local potential model [28] and the Faddeev theory [20]. The *ab initio* calculations such as the anti-symmetrized molecular dynamics [35], the fermionic molecular dynamics [36], the no-core shell model [37] and the lattice calculations [38] have also no order parameter in their theoretical frames. To know whether the phase transition from the Wigner phase to the NG phase of BEC is realized, the order parameter of spontaneous symmetry breaking (SSB) should be defined in the frame of theory. Also up to now, no decisive experimental evidence of BEC of α clusters such as superfluidity or quantum vortex has been observed.

The very recent precise experiments [32] reported that the direct three α decays from the Hoyle state is less than 0.043% [33] and 0.047% [34], respectively. Reference [34] noted that this could indicate that the α -condensate interpretation of the Hoyle state is less likely to be correct. However, the likelihood of the BEC cannot be judged by the amount of the 0s state occupation probability of the α clusters because BEC of α clusters could be realized by a smaller but significant amount of condensation probability. The emergence of BEC can only be concluded by investigating the order parameter of the system.

A cluster model, in which the order parameter that characterizes the phase transition from the Wigner phase of normal solid, liquid or gas-like cluster structure to the NG phase of Bose–Einstein α cluster condensate, is defined is highly needed. In such a model, it is essential to treat the Nambu–Goldstone (NG) operators or zero mode operators rigorously for the systems with a *finite* number of bosons like the three α bosons in the Hoyle state. In a previous work [29], we have proposed an α cluster model, in which an order parameter of BEC of α clusters is defined based on quantum field theory with a spontaneous breakdown of the global phase symmetry, and applied it to the Hoyle and excited states above it in ^{12}C , assuming 100% condensation of the three α clusters. In the present paper, we show, with a realistically smaller but significant amount of condensation probability around 70%, that the Hoyle state and the excited states are well understood as a Bose–Einstein condensate of α clusters.

It has been well-known that the α cluster structure persists not only in light nuclei but also in medium-heavy nuclei as well, most typically in the ^{44}Ti region [5, 10–12], where $j-j$ coupling becomes important due to the strong spin-orbit force. The collective motion such as superdeformation, for example, in ^{36}Ar and ^{38}Ar , can also be understood to be caused by clustering [39, 40]. The α cluster structure study around ^{48}Cr in the fp-shell region was done in Refs.[41–43]. The α cluster condensation in sd-shell region up to ^{40}Ca and in heavier nuclei including ^{52}Fe was paid attention in Ref. [44] and Refs. [45–49], respectively. In the present work, we study BEC

of $N\alpha$ clusters with $N = 3\text{--}13$, i.e., ^{12}C , ^{16}O , ^{20}Ne , ^{24}Mg , ^{28}Si , ^{32}S , ^{36}Ar , ^{40}Ca , ^{44}Ti , ^{48}Cr and ^{52}Fe . We show that collective states of the zero mode operators that are new-type soft modes due to BEC of α clusters emerges systematically. In ^{12}C the observed excited 0_3^+ and 0_4^+ states with a well-developed α cluster structure above the Hoyle state can be interpreted as such a type of soft modes of the zero mode operators associated with the SSB of the global phase of the Bose–Einstein condensate of α clusters. This interpretation is in contrast to the traditional interpretations based on the geometrical picture of the α clusters in the configuration space.

The organization of the paper is as follows. In Secs. II and III, the formulation of the present model is given in detail. Section II is devoted to the formulation of a cluster model with an order parameter that characterizes the phase transition from the Wigner phase of the normal α cluster state to the Bose–Einstein condensate of NG phase of *finite* number of α clusters in the frame of quantum field theory. The zero mode operators due to SSB of the global phase is treated rigorously, keeping the canonical commutation relations. Section III is devoted to the formulation of the Bogoliubov–de Gennes equation. In Sec. IV, the electric transition probabilities for the Bose–Einstein condensate states are formulated. In Sec. V, the BEC of three α clusters in ^{12}C , for which many experimental data are available, are studied in detail under an assumption of realistic condensation rate of 70%. In Sec. VI, the energy level structure, wave functions and electric transitions of ^{12}C at various condensation rates of α clusters, including condensation rate of 100%, are investigated. The robustness of the energy level structure for the different condensation rates is shown. In particular, the systematic appearance of the collective states of the zero mode operators is illustrated for different condensation rates. We proceed to the investigations of the BEC of many α clusters from ^{16}O to ^{52}Fe in Sec. VII. There it is emphasized that the zero mode states of the Nambu–Goldstone mode due to BEC of α clusters is a new kind of soft mode, which appears even in the highly excited energy region in contrast to the concept of the traditional concept of soft mode such as a quadrupole collective motion in the low excitation energy region. We analyze the eigenequation to determine the zero mode states in some detail, and clarify the robustness of the spectra of the zero mode states for various condensation rate and number of α clusters. Summary is given in Sec. VIII.

II. MODEL AND FORMULATION

The formulation was originally presented for BEC of trapped cold atoms in Ref. [29] and is called the interacting zero mode formulation (IZMF in short). The reason for IZMF is explained as follows: The canonical commutation relations of the field operator do not allow us to disregard the zero mode operators in finite-size systems

such as in the trapped cold atomic systems and nuclei, which is associated with the spontaneously broken symmetry, whereas they can be suppressed for homogeneous systems because of their point like contributions in continuum. Once the zero mode operators, denoted by \hat{Q} and \hat{P} , are present, a naive choice of the bilinear unperturbed Hamiltonian leads to the difficulties that no stationary vacuum exists and that the phase of the order parameters should diffuse. To avoid the difficulties, we take the nonlinear unperturbed Hamiltonian of \hat{Q} and \hat{P} . The crucial point for our analysis on α cluster states is that this nonlinear Hamiltonian adds a new type of discrete energy levels with 0^+ to the levels of the Bogoliubov–de Gennes (BdG) modes with various J^P . The combined spectrum of both levels reproduces the observed energy levels above the Hoyle state in ^{12}C very well, by adjusting a single newly introduced parameter of our phenomenological model, the strength of the trapping potential.

As in Ref. [29], we start with the phenomenological model in which the α particles are trapped inside the nuclei by the external isotropic harmonic potential,

$$V_{\text{ex}}(r) = \frac{1}{2}m\Omega^2 r^2, \quad (1)$$

and the α – α interaction is given by the Ali–Bodmer potential [50],

$$U(|\mathbf{x} - \mathbf{x}'|) = V_r e^{-\mu_r^2 |\mathbf{x} - \mathbf{x}'|^2} - V_a e^{-\mu_a^2 |\mathbf{x} - \mathbf{x}'|^2}. \quad (2)$$

The repulsive Coulomb potential affects numerical results very little and is suppressed in this work.

Let $\psi(x)$ ($x = (\mathbf{x}, t)$) be the field operator of the α cluster, and the model Hamiltonian is

$$\begin{aligned} \hat{H} = & \int d^3x \hat{\psi}^\dagger(x) \left(-\frac{\nabla^2}{2m} + V_{\text{ex}}(\mathbf{x}) - \mu \right) \hat{\psi}(x) \\ & + \frac{1}{2} \int d^3x d^3x' \hat{\psi}^\dagger(x) \hat{\psi}^\dagger(x') U(|\mathbf{x} - \mathbf{x}'|) \hat{\psi}(x') \hat{\psi}(x), \end{aligned} \quad (3)$$

where m and μ denote the mass of the α cluster and the chemical potential, respectively. We set $\hbar = c = 1$ throughout this paper. The total Hamiltonian \hat{H} possesses the global phase symmetry, namely that \hat{H} is invariant under $\hat{\psi} \rightarrow e^{i\theta} \hat{\psi}$ with a constant θ . When the α clusters are condensed, the original field operator $\hat{\psi}$ must be divided into a condensate c -number component ξ and an excitation component $\hat{\varphi}$, $\hat{\psi} = \xi + \hat{\varphi}$, according to that the criterion $\langle 0 | \hat{\psi} | 0 \rangle = \xi$. It is vital for our formulation that the function ξ , called the order parameter, is given by the vacuum expectation value of the field operator. Note that the original gauge symmetry is spontaneously broken. The function ξ is assumed to be stationary and isotropic in this paper, and is normalized to the condensed particle number N_0 as $\int d^3x |\xi(\mathbf{x})|^2 = N_0$. Any constant phase of ξ is allowed, refelcting the original global phase symmetry, and as physical results are not affected by its choice, we take a real ξ throughout

this paper. The Hamiltonian (3) is classified according to power degree of $\hat{\varphi}$:

$$\begin{aligned} \hat{H} = & \hat{H}_2 + \hat{H}_{3,4} \\ \hat{H}_2 = & \frac{1}{2} \int d^3x d^3x' \hat{\Phi}(x) \mathcal{T}(\mathbf{x}, \mathbf{x}') \hat{\Phi}(x'), \end{aligned} \quad (4)$$

$$\begin{aligned} \hat{H}_{3,4} = & \frac{1}{2} \int d^3x d^3x' U(|\mathbf{x} - \mathbf{x}'|) \\ & \times [\{2\xi(\mathbf{x}') + \hat{\varphi}^\dagger(x')\} \hat{\varphi}^\dagger(x) \hat{\varphi}(x) \hat{\varphi}(x') + \text{h.c.}], \end{aligned} \quad (5)$$

with $t = t'$, and

$$V_H(\mathbf{x}) = \int d^3x' U(|\mathbf{x} - \mathbf{x}'|) \xi^2(\mathbf{x}'), \quad (6)$$

$$\hat{\Phi}(x) = \begin{pmatrix} \hat{\varphi}(x) \\ \hat{\varphi}^\dagger(x) \end{pmatrix}, \quad \hat{\hat{\Phi}}(x) = \hat{\Phi}^\dagger(x) \sigma_3, \quad (7)$$

$$\mathcal{T}(\mathbf{x}, \mathbf{x}') = \begin{pmatrix} \mathcal{L}(\mathbf{x}, \mathbf{x}') & \mathcal{M}(\mathbf{x}, \mathbf{x}') \\ -\mathcal{M}(\mathbf{x}, \mathbf{x}') & -\mathcal{L}(\mathbf{x}, \mathbf{x}') \end{pmatrix}, \quad (8)$$

$$\mathcal{M}(\mathbf{x}, \mathbf{x}') = U(|\mathbf{x} - \mathbf{x}'|) \xi(\mathbf{x}) \xi(\mathbf{x}'), \quad (9)$$

$$\begin{aligned} \mathcal{L}(\mathbf{x}, \mathbf{x}') = & \delta(\mathbf{x} - \mathbf{x}') \{ -\nabla^2/2m + V_{\text{ex}}(\mathbf{x}) \\ & - \mu + V_H(\mathbf{x}) \} + \mathcal{M}(\mathbf{x}, \mathbf{x}'), \end{aligned} \quad (10)$$

where σ_i ($i = 1, 2, 3$) is the Pauli matrix. We have the Gross–Pitaevskii (GP) equation [51]

$$\{ -\nabla^2/2m + V_{\text{ex}}(\mathbf{x}) - \mu + V_H(\mathbf{x}) \} \xi(\mathbf{x}) = 0, \quad (11)$$

because the $\hat{\varphi}$ -linear term in \hat{H} must vanish, otherwise the ground state could not be stationary.

The field operator $\hat{\varphi}$ is expanded by the complete set of the BdG eigenfunctions,

$$\int d^3x' \mathcal{T}(\mathbf{x}, \mathbf{x}') \mathbf{y}_n(\mathbf{x}') = \omega_n \mathbf{y}_n(\mathbf{x}), \quad (12)$$

$$\mathbf{y}_n(\mathbf{x}) = \begin{pmatrix} u_n(\mathbf{x}) \\ v_n(\mathbf{x}) \end{pmatrix}. \quad (13)$$

The index $\mathbf{n} = (n, \ell, m)$ is a triad of the main, azimuthal, and magnetic quantum numbers for isotropic ξ . Similarly as the BdG equation is introduced for fermionic systems, Eq. (13) is the BdG equation for bosonic systems. The bosonic eigenfunction is normalized as $\int d^3x (|u_n|^2 - |v_n|^2) = 1$ (see Eq. (16)) for the commutation relations, while the fermionic eigenfunction is normalized as $\int d^3x (|u_n|^2 + |v_n|^2) = 1$ for the anti-commutation relations.

Another eigenfunction, denoted by \mathbf{z}_n , is introduced:

$$\int d^3x' \mathcal{T}(\mathbf{x}, \mathbf{x}') \mathbf{z}_n(\mathbf{x}') = -\omega_n \mathbf{z}_n(\mathbf{x}), \quad (14)$$

$$\mathbf{z}_n(\mathbf{x}) = \sigma_1 \mathbf{y}_n^*(\mathbf{x}) = \begin{pmatrix} v_n^*(\mathbf{x}) \\ u_n^*(\mathbf{x}) \end{pmatrix}. \quad (15)$$

The inner product is defined as $((\mathbf{a}, \mathbf{b})) \equiv \int d^3x \mathbf{a}^\dagger(\mathbf{x}) \sigma_3 \mathbf{b}(\mathbf{x})$, and the orthonormal relations are

$$((\mathbf{y}_n, \mathbf{y}_{n'})) = -((\mathbf{z}_n, \mathbf{z}_{n'})) = \delta_{nn'}, \quad (16)$$

$$((\mathbf{y}_n, \mathbf{z}_{n'})) = 0. \quad (17)$$

We also have the eigenfunction with zero eigenvalue,

$$\int d^3x' \mathcal{T}(\mathbf{x}, \mathbf{x}') \mathbf{y}_0(\mathbf{x}') = 0, \quad \mathbf{y}_0(r) = \begin{pmatrix} \xi(\mathbf{x}) \\ -\xi(\mathbf{x}) \end{pmatrix}, \quad (18)$$

which is orthogonal to all the eigenfunctions including itself,

$$((\mathbf{y}_0, \mathbf{y}_0)) = ((\mathbf{y}_0, \mathbf{y}_n)) = ((\mathbf{y}_0, \mathbf{z}_n)) = 0. \quad (19)$$

For the completeness of the set of BdG eigenfunctions, the adjoint eigenfunction \mathbf{y}_{-1} is necessary,

$$\int d^3x' \mathcal{T}(\mathbf{x}, \mathbf{x}') \mathbf{y}_{-1}(\mathbf{x}') = I \mathbf{y}_0(\mathbf{x}), \quad (20)$$

$$\mathbf{y}_{-1}(\mathbf{x}) = \begin{pmatrix} \eta(\mathbf{x}) \\ \eta(\mathbf{x}) \end{pmatrix}, \quad (21)$$

$$((\mathbf{y}_{-1}, \mathbf{y}_{-1})) = ((\mathbf{y}_{-1}, \mathbf{y}_n)) = ((\mathbf{y}_{-1}, \mathbf{z}_n)) = 0, \quad (22)$$

where the constant I is determined by the condition,

$$((\mathbf{y}_{-1}, \mathbf{y}_0)) = 1. \quad (23)$$

The function $\eta(\mathbf{x})$ and the constant I can also be calculated as

$$\eta(\mathbf{x}) = \frac{\partial \xi(\mathbf{x})}{\partial N_0}, \quad I = \frac{\partial \mu}{\partial N_0}. \quad (24)$$

The completeness relation reads as

$$\begin{aligned} \sigma_3 \delta(\mathbf{x} - \mathbf{x}') &= \mathbf{y}_0(\mathbf{x}) \mathbf{y}_{-1}^\dagger(\mathbf{x}') + \mathbf{y}_{-1}(\mathbf{x}) \mathbf{y}_0^\dagger(\mathbf{x}') \\ &+ \sum_n \{ \mathbf{y}_n(\mathbf{x}) \mathbf{y}_n^\dagger(\mathbf{x}') - \mathbf{z}_n(\mathbf{x}) \mathbf{z}_n^\dagger(\mathbf{x}') \}, \end{aligned} \quad (25)$$

and the field operators are expanded as

$$\begin{aligned} \hat{\Phi}(x) &= -i\hat{Q}(t) \mathbf{y}_0(x) + \hat{P}(t) \mathbf{y}_{-1}(x) \\ &+ \sum_n \{ \hat{a}_n(t) \mathbf{y}_n(x) + \hat{a}_n^\dagger(t) \mathbf{z}_n(x) \}, \end{aligned} \quad (26)$$

where the commutation relations,

$$[\hat{Q}, \hat{P}] = i, \quad [\hat{a}_n, \hat{a}_{n'}^\dagger] = \delta_{nn'}, \quad (27)$$

are derived from the canonical commutation relations of $\hat{\varphi}(x)$.

The inevitable appearance of the eigenfunction with zero eigenvalue $\mathbf{y}_0(\mathbf{x})$ and the pair of canonical operators \hat{Q} and \hat{P} is concluded from a general argument using the NG theorem. For this, we derive the Ward-Takahashi relation, adding a symmetry breaking term $-\epsilon \int d^3x \{ \hat{\psi}(x) + \hat{\psi}^\dagger(x) \}$ with an infinitesimal parameter ϵ to the total Hamiltonian \hat{H} in Eq. (3) [52],

$$\begin{aligned} -2\xi(\mathbf{x}) &= -i\epsilon \int d^4y \\ \langle 0 | \text{T} \left[\left\{ \hat{\varphi}_H(y) + \hat{\varphi}_H^\dagger(y) \right\} \left\{ \hat{\varphi}_H(x) - \hat{\varphi}_H^\dagger(x) \right\} \right] | 0 \rangle, \end{aligned} \quad (28)$$

where the suffix H represents the Heisenberg operator. When ξ is a constant, Eq. (28), with the spectral form of the full propagator, leads to the existence of a gapless mode in zero momentum limit in the Fourier space, which is well-known as the NG theorem for a homogeneous system. Equation (28) for the present inhomogeneous system indicates that there should exist an eigenfunction, whose components are proportional to $\xi(\mathbf{x})$. This implies the existence of $\mathbf{y}_0(\mathbf{x})$, having zero eigenvalue, and subsequently the existence of $\mathbf{y}_{-1}(\mathbf{x})$, as above. Then we are forced to introduce \hat{Q} and \hat{P} in the expansion of the field operator. This is an implication of the NG theorem for an inhomogeneous system.

This way the pair of canonical operators \hat{Q} and \hat{P} originate from the SSB of the global phase, and we call them the zero mode operators or NG operators. As was explained in Ref. [29, 53], the substitution of Eq. (26) into Eq. (4) gives $\hat{H}_2 = I\hat{P}^2/2 + \sum_n \omega_n \hat{a}_n^\dagger \hat{a}_n$, whose NG operator part causes serious defects. To avoid the defects, we replace the term $I\hat{P}^2/2$ in the unperturbed Hamiltonian with

$$\begin{aligned} \hat{H}_u^{QP} &= -(\delta\mu + 2C_{2002} + 2C_{1111}) \hat{P} + \frac{I - 4C_{1102}}{2} \hat{P}^2 \\ &+ 2C_{2011} \hat{Q} \hat{P} \hat{Q} + 2C_{1102} \hat{P}^3 + \frac{1}{2} C_{2020} \hat{Q}^4 - 2C_{2011} \hat{Q}^2 \\ &+ C_{2002} \hat{Q} \hat{P}^2 \hat{Q} + \frac{1}{2} C_{0202} \hat{P}^4, \end{aligned} \quad (29)$$

where

$$\begin{aligned} C_{ijj'j'} &= \int d^3x d^3x' U(|\mathbf{x} - \mathbf{x}'|) \\ &\times \{ \xi(\mathbf{x}) \}^i \{ \eta(\mathbf{x}) \}^j \{ \xi(\mathbf{x}') \}^{i'} \{ \eta(\mathbf{x}') \}^{j'}, \end{aligned} \quad (30)$$

and $\delta\mu$ is a counter term that the criterion $\langle 0 | \hat{\psi} | 0 \rangle = \xi$ determines. The Hamiltonian H_u^{QP} is obtained from gathering all the terms consisting only of \hat{Q} and \hat{P} in \hat{H}_2 and $\hat{H}_{3,4}$. We set up the eigenequation of H_u^{QP} ,

$$\hat{H}_u^{QP} |\Psi_\nu\rangle = E_\nu |\Psi_\nu\rangle \quad (\nu = 0, 1, \dots). \quad (31)$$

The eigenstates $\{ |\Psi_\nu\rangle \}$ are collective states of \hat{Q} and \hat{P} , simply called *zero mode states*, and span their own state subspace, referred to as the NG subspace. The state of the total system $|\mathcal{S}\rangle$ is expressed as a direct product,

$$|\mathcal{S}\rangle = |\Psi_\nu\rangle |\cdot\rangle_{\text{ex}}, \quad (32)$$

where $|\cdot\rangle_{\text{ex}}$ is a Fock state associated with the BdG mode operator \hat{a}_n . The discrete spectrum of the zero mode states in Eq.(31) is our original consequence that is to be compared with the observed energy levels. We may point out a resemblance between the breakings of the rotational symmetry in the deformed nuclear ground state [2] and the global phase symmetry in our model. Because both are SSBs in finite systems, the quantum degrees of freedom to restore the broken symmetries appear as the zero mode operators, which give rise to a rotational band

of the states in case of the broken rotational symmetry and the collective states $|\Psi_\nu\rangle$ with E_ν in our present case.

The vacuum state $|\Psi_0\rangle|0\rangle_{\text{ex}}$ is identified as the Hoyle state just above the three α threshold in the case of ^{12}C . The states $|\Psi_\nu\rangle|0\rangle_{\text{ex}}$ ($\nu = 1, 2, \dots$), are NG (or zero mode) excited states with the excitation energy from the vacuum $E_\nu - E_0$. The excitation in the NG subspace changes neither the value of the angular momentum J nor the sign of the parity P . The state $|\Psi_0\rangle(\hat{a}_n^\dagger|0\rangle_{\text{ex}})$, called the BdG state, has the excitation energy ω_n , measured from the vacuum state.

III. BOGOLIUBOV-DE GENNES EQUATION

We give the BdG equations here in some details which were not presented explicitly in Ref. [29]. We put the following separable form of the BdG eigenfunction in Eq. (13),

$$\mathbf{y}_n(\mathbf{x}) = \begin{pmatrix} \mathcal{U}_{n\ell}(r) \\ \mathcal{V}_{n\ell}(r) \end{pmatrix} Y_{\ell m}(\theta, \varphi). \quad (33)$$

For convenience the function $\tilde{U}_{\ell m}(r, r', \theta, \varphi)$ is introduced as

$$\begin{aligned} \tilde{U}_{\ell m}(r, r', \theta, \varphi)/r'^2 \equiv \\ \int d\Omega' U(\sqrt{r^2 + r'^2 - 2rr'\cos(\theta' - \theta)}) Y_{\ell m}(\theta', \varphi'). \end{aligned} \quad (34)$$

For performing the surface integral, the direction of the z' -axis is taken along the vector \mathbf{x} and then $\cos(\theta' - \theta)$ becomes $\cos\theta'$. We define the eigenfunctions of $\hat{L}_n = \hat{\mathbf{L}} \cdot \mathbf{x}/r$, denoted by $Y_{\ell m}^n(\theta, \varphi)$, as $\hat{L}_n Y_{\ell m}^n(\theta, \varphi) = m Y_{\ell m}^n(\theta, \varphi)$. The Wigner D -matrix gives the following relations,

$$Y_{\ell m}^n(\theta', \varphi') = \sum_{m'} D_{m'm}^{\ell,*}(\varphi, \theta, 0) Y_{\ell m'}(\theta', \varphi'), \quad (35)$$

$$Y_{\ell m}(\theta', \varphi') = \sum_{m'} D_{mm'}^\ell(\varphi, \theta, 0) Y_{\ell m'}^n(\theta', \varphi'). \quad (36)$$

The last relation is substituted into Eq. (34), and we integrate it over the variable φ' to have

$$\begin{aligned} \tilde{U}_{\ell m}(r, r', \theta, \varphi)/r'^2 = 2\pi Y_{\ell m}(\theta, \varphi) \\ \times \int_{-1}^1 dw U(\sqrt{r^2 + r'^2 - 2rr'w}) P_\ell(w), \end{aligned} \quad (37)$$

where the relation $D_{m0}^\ell(\varphi, \theta, 0) = \sqrt{\frac{4\pi}{2\ell+1}} Y_{\ell m}(\theta, \varphi)$ has been used. For the isotropic $\xi(\mathbf{x}) = \xi(r)$, V_H in Eq. (6) is also isotropic, given by

$$V_H(r) = \frac{N_0}{\sqrt{4\pi}} \int dr' \tilde{U}_{00}(r, r') \tilde{\xi}^2(r'), \quad (38)$$

where

$$\xi(r) = \sqrt{\frac{N_0}{4\pi}} \tilde{\xi}(r), \quad (39)$$

$$\begin{aligned} \tilde{U}_{00}(r, r') = \frac{\sqrt{\pi} r'}{r} \left\{ \frac{V_r}{2\mu_r^2} \left(e^{-\mu_r^2(r-r')^2} - e^{-\mu_r^2(r+r')^2} \right) \right. \\ \left. - \frac{V_a}{2\mu_a^2} \left(e^{-\mu_a^2(r-r')^2} - e^{-\mu_a^2(r+r')^2} \right) \right\}. \end{aligned} \quad (40)$$

The Fock term in Eq. (12) is manipulated as

$$\begin{aligned} \int d^3x' \mathcal{M}(\mathbf{x}, \mathbf{x}') u_n(\mathbf{x}') \\ = \frac{N_0}{4\pi} \tilde{\xi}(r) \int dr' \tilde{\xi}(r') \mathcal{U}_{n\ell}(r') \tilde{U}_{\ell m}(r, r', \theta, \varphi) \\ = F_\ell[r : \mathcal{U}_{n\ell}] \tilde{\xi}(r) Y_{\ell m}(\theta, \varphi) \end{aligned} \quad (41)$$

with a linear functional of f ,

$$\begin{aligned} F_\ell[r : f] = \frac{N_0}{2} \int dr' r'^2 \tilde{\xi}(r') f(r') \\ \times \int_{-1}^1 dw U(\sqrt{r^2 + r'^2 - 2rr'w}) P_\ell(w), \end{aligned} \quad (42)$$

and similarly for v_n . The BdG equation (12) is reduced to

$$h_\ell \mathcal{U}_{n\ell}(r) + F_\ell[r : \mathcal{U}_{n\ell} + \mathcal{V}_{n\ell}] \tilde{\xi}(r) = \omega_n \mathcal{U}_{n\ell}(r), \quad (43)$$

$$h_\ell \mathcal{V}_{n\ell}(r) + F_\ell[r : \mathcal{U}_{n\ell} + \mathcal{V}_{n\ell}] \tilde{\xi}(r) = -\omega_n \mathcal{V}_{n\ell}(r), \quad (44)$$

with

$$\begin{aligned} h_\ell = -\frac{1}{2m} \left(\frac{d^2}{dr^2} + \frac{2}{r} \frac{d}{dr} - \frac{\ell(\ell+1)}{r^2} \right) \\ + V_{\text{ex}}(r) - \mu + V_H(r). \end{aligned} \quad (45)$$

IV. ELECTRIC TRANSITION PROBABILITIES

The formulation presented in Secs. II and III enables us to calculate the γ -decay transitions among the states with α cluster condensate.

The decay rate of an electric transition with a photon angular momentum J for an unpolarized initial state and summing all final polarization states [1] is generally given by

$$\bar{\Gamma}_{fi}(\mathbf{E} : k, J) = \frac{8\pi(J+1)}{J((2J+1)!!)^2} k^{2J+1} B(\mathbf{E}J : J_i \rightarrow J_f), \quad (46)$$

where k is the photon energy $k = E_i - E_f$, calculated from the initial and final state energies of the nucleus E_i and E_f . The symbol B stands for the reduced transition probability,

$$\begin{aligned} B(\mathbf{E}J : J_i \rightarrow J_f) = \\ \frac{1}{2J_i + 1} \left| \langle f(J_f) | | \hat{\mathcal{M}}(\mathbf{E} : kJ) | | i(J_i) \rangle \right|^2, \end{aligned} \quad (47)$$

where $\hat{\mathcal{M}}$ is the multipole moment, and $|i\rangle$, $|j\rangle$, J_i , and J_f are the initial and final nuclear states and spins, respectively.

The transitions, $|\Psi_0\rangle(\hat{a}_{12m}^\dagger|0\rangle_{\text{ex}}) \rightarrow |\Psi_0\rangle|0\rangle_{\text{ex}}$ and $|\Psi_1\rangle|0\rangle_{\text{ex}}$, correspond in our approach to the transitions, $2_2^+ \rightarrow 0_2^+$ and 0_3^+ in ^{12}C , respectively, which will be discussed in the next sections. The reduced transition probabilities for these processes are calculated as

$$B(\text{E}2 : 2 \rightarrow 0) = \left| \langle f(J_f = 0, M_f = 0) | \hat{\mathcal{M}}(\text{E} : k20) | i(J_i = 2, M_i = 0) \rangle \right|^2, \quad (48)$$

and we have for $2_2^+ \rightarrow 0_2^+$

$$\begin{aligned} \langle f(0, 0) | \hat{\mathcal{M}}(\text{E} : k20) | i(2, 0) \rangle = & \\ & \frac{60e\sqrt{N_0}}{mk^3} \int dr r \left[\tilde{\xi}(r) \left\{ \frac{d}{dr} \mathcal{U}_{12}(r) j_2(kr) \right. \right. \\ & + \mathcal{U}_{12}(r) \left(\frac{j_2(kr)}{r} + k j_2'(kr) \right) \left. \right\} \\ & + \left. \frac{d}{dr} \tilde{\xi}(r) \mathcal{V}_{12}(r) j_2(kr) \right], \quad (49) \end{aligned}$$

and for $2_2^+ \rightarrow 0_3^+$

$$\begin{aligned} \langle f(0, 0) | \hat{\mathcal{M}}(\text{E} : k20) | i(2, 0) \rangle = & \\ & \frac{60e\sqrt{N_0}}{mk^3} \int dr r \left[\left\{ i \langle \Psi_1 | \hat{Q} | \Psi_0 \rangle \tilde{\xi}(r) + \langle \Psi_1 | \hat{P} | \Psi_0 \rangle \tilde{\eta}(r) \right\} \right. \\ & \times \left\{ \frac{d}{dr} \mathcal{U}_{12}(r) j_2(kr) + \mathcal{U}_{12}(r) \left(\frac{j_2(kr)}{r} + k j_2'(kr) \right) \right\} \\ & + \left\{ i \langle \Psi_1 | \hat{Q} | \Psi_0 \rangle \frac{d}{dr} \tilde{\xi}(r) + \langle \Psi_1 | \hat{P} | \Psi_0 \rangle \frac{d}{dr} \tilde{\eta}(r) \right\} \\ & \left. \times \mathcal{V}_{12}(r) j_2(kr) \right], \quad (50) \end{aligned}$$

where j_ℓ is the spherical Bessel function and $j'_\ell(z) = \frac{dj_\ell}{dz}$, and $\eta(\mathbf{x}) = \eta(r) = \sqrt{\frac{N_0}{4\pi}} \tilde{\eta}(r)$.

The monopole E0 transition probabilities for the processes $0_2^+ \rightarrow 0_3^+$ and 0_4^+ are given by

$$\begin{aligned} M(\text{E}0 : 0_2^+ \rightarrow 0_{\nu+2}^+) &= \left| \langle \Psi_\nu | 2e \int d^3x \hat{\psi}^\dagger(\mathbf{x}) \hat{\psi}(\mathbf{x}) | \Psi_0 \rangle \right|^2 \\ &= 4e^2 \left| I_{QQ} \langle \Psi_\nu | \hat{Q}^2 | \Psi_0 \rangle + I_{PP} \langle \Psi_\nu | \hat{P}^2 | \Psi_0 \rangle \right. \\ & \quad \left. + I_P \langle \Psi_\nu | \hat{P} | \Psi_0 \rangle \right|^2, \quad (51) \end{aligned}$$

where $\nu = 1, 2$ and

$$\begin{aligned} I_{QQ} &= \int d^3x r^2 \xi^2(\mathbf{x}), \quad I_{PP} = \int d^3x r^2 \eta^2(\mathbf{x}), \\ I_P &= 2 \int d^3x r^2 \xi(\mathbf{x}) \eta(\mathbf{x}). \quad (52) \end{aligned}$$

TABLE I. The fitted parameters of Ω and V_r for three rms radius \bar{r} of ^{12}C with $N_0 = 0.7N$.

\bar{r} [fm]	Ω [MeV]	V_r [MeV]	common parameters
3.8	2.42	415	$V_a = 130$ MeV
3.5	2.84	398	$\mu_a = 0.475$ fm $^{-1}$
3.2	3.38	380	$\mu_r = 0.7$ fm $^{-1}$

V. BOSE-EINSTEIN CONDENSATION OF ALPHA CLUSTERS IN ^{12}C : REALISTIC 70% CONDENSATION CASE

First we study the BEC of α clusters in the Hoyle state at 7.654 MeV excitation energy of ^{12}C and the excited states above it. Using a three α cluster orthogonality condition model, Yamada and Schuck [54] confirmed the result of Matsumura and Suzuki [25] that about 70% of the three α particles in the Hoyle state are sitting in the 0s state. Here it is to be noted that this large probability 70% itself, compared to a superfluid liquid HeII, does not necessarily mean the realization of the BEC of three α clusters. Because these traditional cluster models do not have an order parameter to characterize the phase transition in its theory, it is impossible to judge in principle whether the system is in the NG phase with its global phase being locked or not. We attempt this 70%, i.e., $N_0 = 0.7N$ in our calculations, investigate whether BEC is realized for the $N = 3$ system.

A. Alpha-alpha and trapping potentials

The original nuclear force is supposed to fill the two separate roles in our phenomenological approach: One is to trap the α clusters inside the nucleus, represented by the external harmonic potential $V_{ex}(r)$ in Eq. (1) with the parameter Ω . The other is a residual α - α interaction, for which we take the Ali-Bodmer potential $U(r)$ in Eq. (2) for the s -wave, which is specified by the four parameters, the strengths of the repulsive and attractive parts, V_r and V_a , and their respective inverse ranges, μ_r and μ_a [50]. These four parameters have been determined to fit the phase shifts of α - α scattering [50].

In the present calculations we adjust V_r , which is the most sensitive to our analysis among the four parameters, while the remaining parameters are kept fixed. The used potential parameter set d_0 of Ref. [50] are $V_a = 130$ MeV, $\mu_a = 0.475$ fm $^{-1}$, and $\mu_r = 0.7$ fm $^{-1}$. The two parameters Ω and V_r play the role to balance between concentration by $V_{ex}(r)$ and repulsion by $U(r)$, which are crucial for a stable condensate.

The vacuum state $|\Psi_0\rangle|0\rangle_{\text{ex}}$ is identified as the Hoyle state in the calculations. The rms radius of the Hoyle state, denoted by $\bar{r} = \sqrt{\langle r^2 \rangle}$, is calculated from $\xi(r)$. As the α cluster model calculations [21–23, 25, 35] report the range of $\bar{r} = 3.2$ –3.8 fm typically, we consider the three cases of $\bar{r} = 3.8$, 3.5 and 3.2 fm. The two parameters Ω

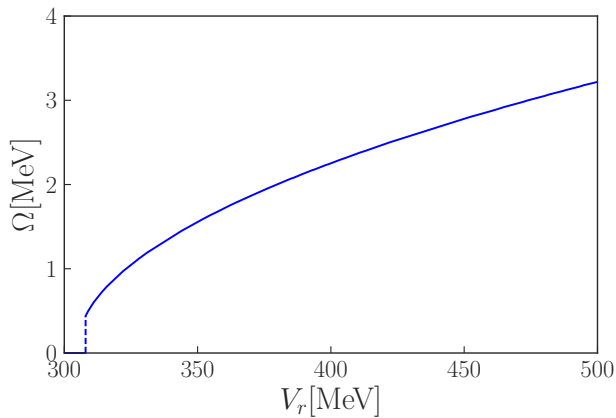


FIG. 1. (Color online) The relation between the confining potential parameter Ω and the repulsive potential V_r for ^{12}C is plotted for the case of $\bar{r} = 3.8$ fm with $N_0 = 0.7N$. As shown by the vertical dashed lines, the BEC system collapses for V_r smaller than the critical value around 310 MeV.

and V_r are determined to reproduce the experimental 0_3^+ state, i.e., the first 0^+ state above the Hoyle state, which is considered to be the first NG excited state $|\Psi_1\rangle|0\rangle_{\text{ex}}$. The parameters Ω and V_r are given in Table I when $N_0 = 0.7N$ is assumed.

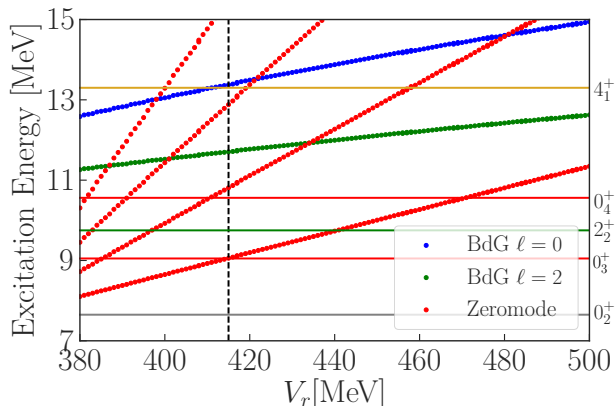


FIG. 2. (Color online) The energy levels of ^{12}C calculated with $N_0 = 0.7N$ as a function of V_r for $\bar{r} = 3.8$ fm are compared with the observed energy levels (horizontal lines) taken from Refs. [30, 31, 55–58].

Figure 1 shows how Ω and V_r are constrained when \bar{r} is fixed to be 3.8 fm. An increase in Ω requires an increase in V_r to keep a constant \bar{r} , and they are related roughly as $\Omega^2 \propto V_r$. As is noted in Ref. [29] where 100% condensation was assumed, we see in Fig. 1 that the BEC for the $N_0 = 0.7N$ case also becomes unstable when V_r is smaller than some critical value. As displayed in Fig. 2, the parameters are determined to reproduce the experimental excitation energy of 0_3^+ from the vacuum, $E_1 - E_0$. The parameters in Table I for $\bar{r} = 3.5$ and 3.2 fm are determined similarly.

B. The order parameter, BdG eigenfunctions and wavefunctions of the zero mode states

The calculated wave functions are shown in Figs. 3–5 in sequence.

The eigenfunction with zero eigenvalue in Eq. (18) or the order parameter in Eq. (11), $\xi(r)$, is shown in Fig. 3 (a). In Fig. 3 (b) the adjoint eigenfunction $\eta(r)$ in Eq. (21), which is calculated as a derivative of ξ with respect to the number of the α clusters N_0 in Eq. (24), represents the fluctuation of the number of α clusters [62]. The $|\xi(r)|^2$ represents the condensate fraction density, and the superfluid density [59–61] is given by $|\xi(r)|^2/N_0$. In Fig. 3 (c) the radial density distribution of the condensate, defined by $r^2\xi^2(r)/N_0$ is displayed. We see from Fig. 3 (a) that the superfluid density distribution of the condensate α clusters in the vacuum Hoyle state extends to about 8 fm, which is consistent with the picture of the diffused gas-like structure. As the size of the condensate becomes larger from $\bar{r} = 3.2$ to 3.8 fm, the density in the central region is depressed while that in the surface is enhanced. In Fig. 3 (b) we note that the number fluctuation around the average N_0 is roughly flat up to 4 fm with about 0.05, 0.045 and 0.04 for $\bar{r} = 3.8, 3.5$ and 3.2 fm, respectively, and with a small depression at around 2–2.5 fm, and extends to about 8fm. The magnitude of η is considerably large even at 6 fm compared with ξ , which means that the number fluctuation occurs significantly not only in the central region but also in the surface region beyond the rms radius up to about 6 fm. As seen in Fig. 3 (c), the radial distribution of the superfluid density diffuses more widely for larger size of the condensate.

In Fig. 4 the wave functions of the first BdG excitation modes ($n = 1$) with $\ell = 0, 2$ and 4 are shown. The radial behavior of $\mathcal{U}_{1\ell}(r)$, which represents the radial extension of the state, is rather similar to that of ξ in Fig. 3 (a). The peak position of $\mathcal{U}_{1\ell}(r)$ moves outward as ℓ increases. This is reasonably understood by considering that the states with larger ℓ correspond to the higher excitation energy, as seen in Fig. 2. On the other hand, in Fig. 4 we see that $\mathcal{V}_{1\ell}(r)$ is drastically small compared to $\mathcal{U}_{1\ell}(r)$ as ℓ increases and is strongly damped beyond $r = 4$ fm in the surface region for all the cases of $\bar{r} = 3.2 - 3.8$ fm. The size of the condensate is dominantly determined by the behavior of the wave function $\mathcal{U}_{1\ell}(r)$. In fact, as the size of the condensate becomes larger from $\bar{r} = 3.2$ to 3.8 fm, the peak of $\mathcal{U}_{1\ell}(r)$ moves outward and the amplitude at the surface is increased, while that in the internal region decreases. The magnitude of $\mathcal{V}_{1\ell}(r)$, which represents the quantum fluctuations of the α clusters of the condensate, decreases for larger ℓ . For $\ell = 0$ the magnitude of $\mathcal{V}_{10}(r)$ in the internal region is not small compared to $\mathcal{U}_{10}(r)$, which means that the quantum fluctuation is significant for $\ell = 0$. The node of the $\mathcal{U}_{1\ell}(r)$ for $\ell = 0$ is due to the orthogonality to the nodeless ξ and η .

As in Table I, V_r changes only slightly in our fitting, and the wave functions are determined mainly by the

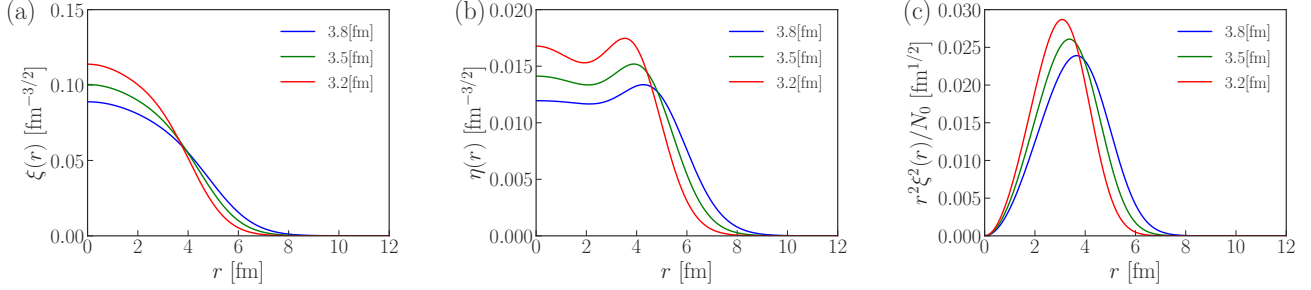


FIG. 3. (Color online) The calculated (a) eigenfunction with zero eigenvalue $\xi(r)$, (b) its adjoint eigenfunction $\eta(r)$ and (c) radial density distribution of the condensate $r^2|\xi(r)|^2/N_0$ for $\bar{r} = 3.8, 3.5$ and 3.2 fm with $N_0 = 0.7N$ in ^{12}C .

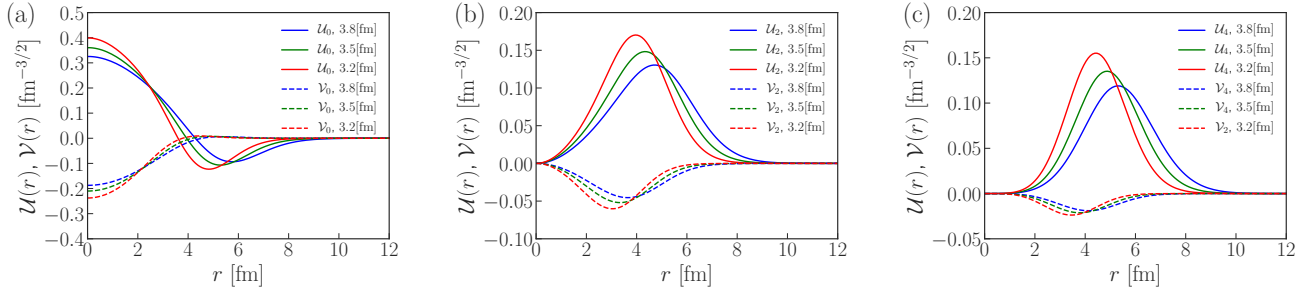


FIG. 4. (Color online) Numerically calculated BdG wavefunctions, $\mathcal{U}_{1\ell}(r)$ (solid lines) and $\mathcal{V}_{1\ell}(r)$ (dashed lines) for (a) $\ell = 0$, (b) $\ell = 2$, and (c) $\ell = 4$ for $\bar{r} = 3.8, 3.5$ and 3.2 fm with $N_0 = 0.7N$ in ^{12}C . In the legends of the figures, the suffix $n = 1$ is omitted and only ℓ is given for $\mathcal{U}_{1\ell}$ and $\mathcal{V}_{1\ell}$.

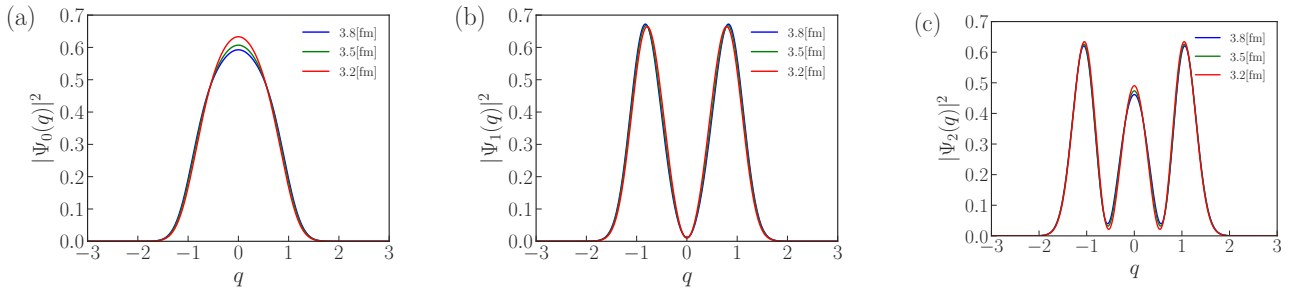


FIG. 5. (Color online) The squares of numerically calculated wavefunctions of the zero mode states, (a) $|\Psi_0(q)|^2$, (b) $|\Psi_1(q)|^2$, and (c) $|\Psi_2(q)|^2$, for $\bar{r} = 3.8, 3.5$ and 3.2 fm with $N_0 = 0.7N$ in ^{12}C .

value of Ω , not by the value of V_r . It is natural, as seen in Figs. 3 and 4, that the peaks at the center are enhanced or the peak positions are shifted closer to the center with the higher peaks, as \bar{r} is smaller. We note the relation $\bar{r} \propto 1/\sqrt{\Omega}$ there, which is identical with the relation for the ground state wave function of a simple harmonic oscillation.

We introduce the eigenstate of \hat{Q} , denoted by $|q\rangle$, as $\hat{Q}|q\rangle = q|q\rangle$. In order to solve Eq. (31), we move to the q -diagonal representation, in which the state is rep-

resented by the wavefunction $\Psi_\nu(q) = \langle q|\Psi_\nu\rangle$, and the operators \hat{Q} and \hat{P} are represented by q and $\frac{1}{i}\frac{\partial}{\partial q}$, respectively, consistently with Eq. (27). Figure 5 represents $|\Psi_\nu(q)|^2$ ($\nu = 0, 1, 2$) numerically calculated. We see that the excitation of the NG mode is caused by the nodal excitation of $\Psi_\nu(q)$ with respect to q in the NG subspace. It is important to note that this nodal excitation is anharmonic as seen in \hat{H}_v^{QP} in Eq. (29), which brings the excitation energy of the $\nu = 1$ state lower and closer to the vacuum, and the $\nu = 2$ state closer to the $\nu = 1$ state

in Fig. 2 (and Fig. 13 later). In fact, in Fig. 2 (Fig. 13) the energy intervals between the $\nu = 0$ and $\nu = 1$ states, and between the $\nu = 1$ and $\nu = 2$ states are smaller than those for other higher NG mode states for $\nu > 2$. It is worth noting that the NG wave functions and the NG excitation energies depend very little on \bar{r} and Ω . This is because the coefficients of \hat{H}_u^{QP} in Eq. (29) include the Ω -dependent $\xi(r)$ and $\eta(r)$ only in the integrands and the integration values are insensitive to Ω . On the other hand, the coefficients of \hat{H}_u^{QP} have a factor V_r , and the NG energy levels rise with an increasing V_r .

C. Electric transition probabilities

Using the obtained wave functions, the reduced transition probabilities in Eq. (47) with Eqs. (48) and (49) and the monopole transition probabilities in Eq. (51) are calculated numerically. The results are summarized in Table II in comparison with other theoretical calculations in Refs. [35] and [24]. There the parameters are $\Omega = 2.42$ MeV and $V_r = 415$ MeV in the case of $\bar{r} = 3.8$ fm in Table I. We note the difference of our results between the E2 transitions $2_2^+ \rightarrow 0_2^+$ and $2_2^+ \rightarrow 0_3^+$: Whereas the former is the transition to change only the BdG state, the latter involves transition in both of the NG and BdG states. The difference between the two monopole transitions $0_2^+ \rightarrow 0_3^+$ and $0_2^+ \rightarrow 0_4^+$ is explained as follows: The most dominant term $I_p \langle \Psi_\nu | \hat{P} | \Psi_0 \rangle$ interferes with the other two terms constructively in the former, but destructively in the latter.

TABLE II. Calculated reduced transition probabilities $B(E2 : 2 \rightarrow 0)$ and monopole transition probabilities $M(E0 : 0 \rightarrow 0)$ in ^{12}C with 70% and 100% (see Subsec. VIB) condensation in units of $e^2 \text{fm}^4$ and fm^2 , respectively, are displayed in comparison with Ref. [35] and Ref. [24].

Transition	70%	100%	Ref. [35]	Ref. [24]
$B(E2 : 2_2^+ \rightarrow 0_2^+)$	121	158	100	295-340
$B(E2 : 2_2^+ \rightarrow 0_3^+)$	76	62	310	88-220
$M(E0 : 0_2^+ \rightarrow 0_3^+)$	1.59	2.34	34.5	2.0
$M(E0 : 0_2^+ \rightarrow 0_4^+)$	0.072	0.145	0.57	—

VI. ROBUSTNESS OF BOSE-EINSTEIN CONDENSATE STRUCTURE OF ^{12}C VS CONDENSATION RATES

So far it has been assumed that the α clusters inside ^{12}C are condensed with $N_0 = 0.7N$ based on the preceding cluster model calculations [25, 54] that about 70% of three α clusters inside ^{12}C are in the 0s state. However, experimentally the condensation rate has not been directly measured. Therefore it seems important to investigate whether the structure obtained under 70% con-

densation is robust for the different condensation rates. Here we study and compare the three cases of condensation, $N_0 = 3.0$ (condensation rate 100%), 2.5 (83%) and 2.0 (67%) in ^{12}C .

A. Three cases of condensation rate: $N_0 = 3, 2.5$ and 2

Similarly as in the previous section, we determine the confining and α - α potentials by adjusting the parameters of Ω and V_r , for different N_0 with $\bar{r} = 3.8$ [fm] and E_1 . The obtained potential parameters are summarized in Table III. The values of Ω and V_r depend only slightly on N_0 .

TABLE III. The fitted parameters of Ω and V_r used in the calculations with different three condensation rates of $N_0 = 3.0, 2.5, 2.0$ in ^{12}C with fixed $\bar{r} = 3.8$ fm.

N_0	Ω [MeV]	V_r [MeV]	common parameters
3.0	2.62	403	$V_a = 130$ MeV
2.5	2.53	410	$\mu_a = 0.475$ fm $^{-1}$
2.0	2.40	417	$\mu_r = 0.7$ fm $^{-1}$

In Fig. 6 the calculated energy levels of ^{12}C for different three condensation rates are displayed. The zero mode excitation levels remain constant or rise only slightly as N_0 becomes smaller. This is because \bar{r} and V_r are fixed and the fitted Ω is therefore almost constant for varying N_0 . This shows that the nature of the low-lying zero mode states just above the Hoyle state, the experimental 0_3^+ and the 0_4^+ states, is robust with respect to the changes of the condensation rates. On the other hand, the BdG excitation energies decrease only slightly as N_0 becomes smaller. This is reasonable because the Hartree and Fock terms of the self-interaction in BdG equations (43) and (44), which push up energy levels due to a dominant contribution of the repulsive force, are proportional to N_0 . This is also understood as follows. Because Ω becomes smaller as N_0 decreases as in Table III, the BdG vibrational energy becomes smaller. As a result, the choice of $N_0 = 2.0$, about 70% condensation, gives the most favorable BdG energy levels in our calculations.

B. Detailed study of 100% condensation case

To see how the energy level structure, wave functions and electric transitions, calculated with $N_0 = 0.7N$ in the previous section, are affected for the different three condensation rates, we will focus on comparing them here with those in the 100% condensation case. A brief result of 100% condensation has been given in Ref.[29]. We will present here the results rather in detail because it was found that there were small errors in numerical calculations involving the BdG modes with $\ell = 2$ and 4,

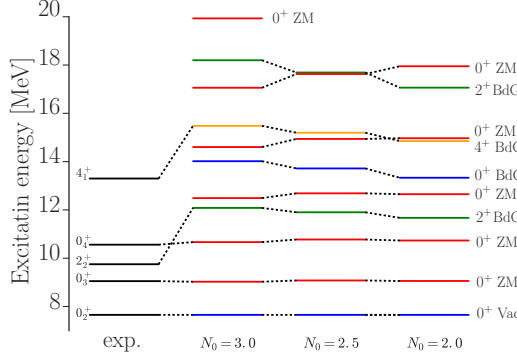


FIG. 6. (Color online) The energy levels of ^{12}C calculated with the parameters in Table III for the three condensation rates, $N_0 = 3.0$ (100%), 2.5 (83%) and 2.0 (67%), with fixed $\bar{r} = 3.8$ fm.

although the results for the zero mode states and the BdG modes with $\ell = 0$ are not altered.

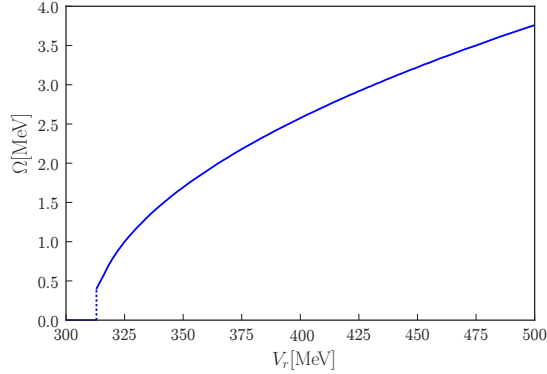


FIG. 7. The relation between the confining potential parameter Ω and the repulsion potential V_r for ^{12}C is plotted for the case of $\bar{r} = 3.8$ fm with 100% condensation ($N_0 = N$).

As shown in Fig. 7, the two parameters Ω and V_r are constrained for $N_0 = N$ when \bar{r} is fixed to be 3.8 fm, similarly to the $N_0 = 0.7N$ case in Fig. 1. The parameters are determined as in Fig. 8, similarly to the 70% case in Fig. 2, and the obtained parameters are given in Table IV.

1. Energy levels

The energy levels, calculated from the parameters in Table IV, are displayed for each of $\bar{r} = 3.8, 3.5, 3.2$ fm in Fig. 9. The 0_4^+ state is reproduced well as the second NG excited state $|\Psi_2\rangle|0\rangle_{\text{ex}}$, which is similar to the $N_0 = 0.7N$ case for the whole calculated range of the \bar{r} . The

calculated levels of the 2_2^+ and 4_1^+ states are identified as the lowest excitations of the BdG modes with $\ell = 2$ and $\ell = 4$, respectively. The BdG energy levels show that the levels increase for smaller \bar{r} . The increase in Ω affects more dominantly on the levels than the decrease in V_r , similarly to the 70% condensation case.

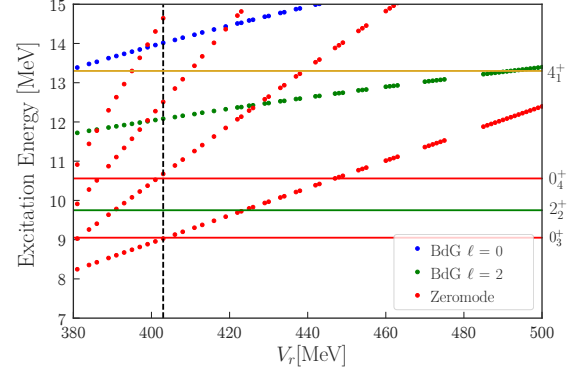


FIG. 8. (Color online) The energy levels of ^{12}C calculated with 100% condensation ($N_0 = N$) as a function of V_r for $\bar{r} = 3.8$ fm are compared with the observed energy levels (horizontal lines) taken from Refs. [30, 31, 55–58].

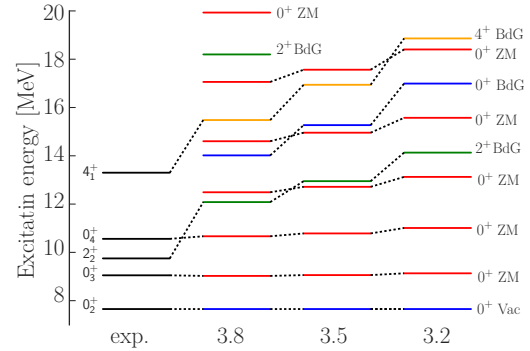


FIG. 9. (Color online) The energy levels of ^{12}C , calculated from the parameters in Table IV with fixed 100% condensation ($N_0 = N$) for $\bar{r} = 3.8, 3.5$ and 3.2 fm, are compared with the experimental energy levels from Refs. [30, 31, 55–58]. Vac, ZM and BdG mean the vacuum Hoyle state, zero mode states and BdG excited states, respectively.

2. The order parameter, BdG eigenfunctions and wavefunctions of the zero mode states

The results of the calculated wave functions with 100% condensation are shown in sequence. The eigenfunction

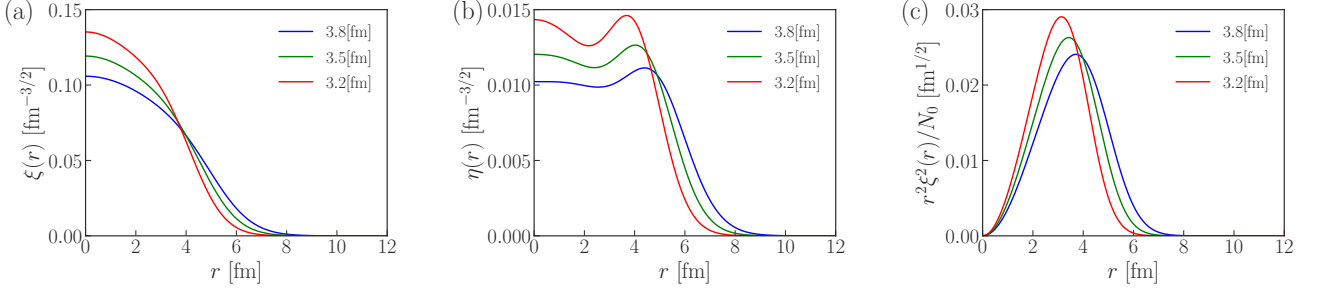


FIG. 10. (Color online) Numerically calculated (a) $\xi(r)$, (b) $\eta(r)$ and (c) the radial density distribution of the condensate $r^2|\xi(r)|^2/N_0$ with $\bar{r} = 3.8, 3.5, 3.2$, fm for 100% condensation ($N_0 = N$).

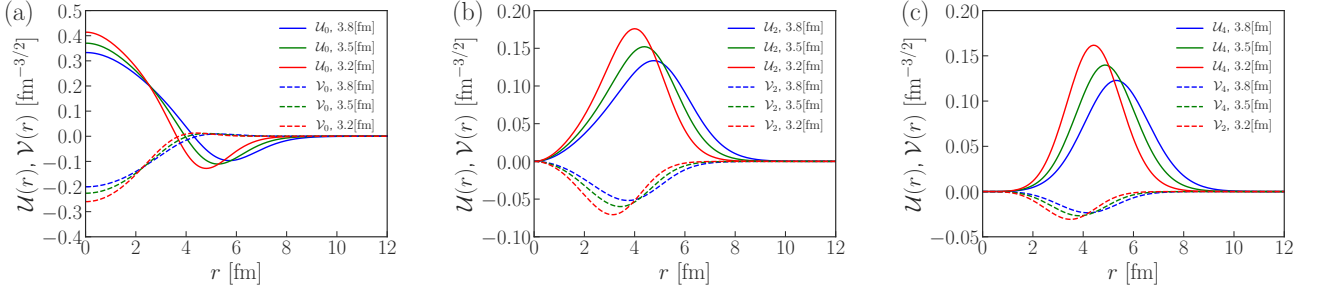


FIG. 11. (Color online) Numerically calculated BdG wavefunctions, $\mathcal{U}_{1\ell}(r)$ (solid lines) and $\mathcal{V}_{1\ell}(r)$ (dashed lines) for (a) $\ell = 0$, (b) $\ell = 2$, and (c) $\ell = 4$, with $\bar{r} = 3.8, 3.5, 3.2$, fm for 100% condensation ($N_0 = N$).

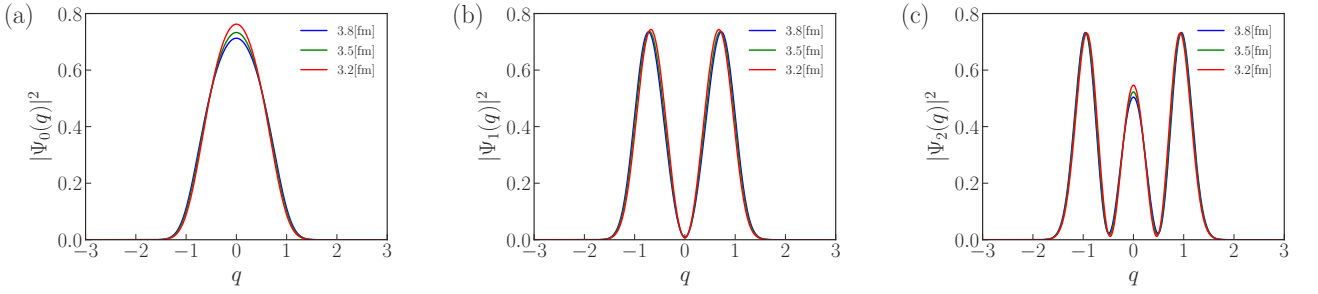


FIG. 12. (Color online) The squares of numerically calculated wavefunctions of the zero mode states, (a) $|\Psi_0(q)|^2$, (b) $|\Psi_1(q)|^2$, and (c) $|\Psi_2(q)|^2$, with $\bar{r} = 3.8, 3.5, 3.2$, fm for 100% condensation ($N_0 = N$).

TABLE IV. The fitted parameters of Ω and V_r for three rms radius $\bar{r} = 3.8, 3.5$ and 3.2 fm of ^{12}C with 100% condensation ($N_0 = N$).

\bar{r} [fm]	Ω [MeV]	V_r [MeV]	common parameters
3.8	2.62	403	$V_a = 130$ MeV $\mu_a = 0.475$ fm $^{-1}$ $\mu_r = 0.7$ fm $^{-1}$
3.5	3.10	389	
3.2	3.77	375	

with zero eigenvalue in Eq. (18) or the order param-

eter in Eq. (11), $\xi(r)$, and its adjoint eigenfunction $\eta(r)$ in Eq. (21) are depicted in Fig. 10 (a) and (b), respectively. The radial density distribution of the condensate is also shown in Fig. 10 (c). By comparing Figs. 3 and 10, we see that the essential features of the behavior of $\xi(r)$ and $\eta(r)$ with $\bar{r} = 3.8, 3.5$ and 3.2 fm change little, irrespective of the condensation rates 70% and 100%. In Fig. 11 the wave functions of the first BdG excitation modes ($n = 1$) with $\ell = 0, 2$ and 4 are displayed. We see that the features of the BdG wave functions there for the three different sizes of the condensate with $\bar{r} = 3.8, 3.5$

and 3.2 fm are similar to those in Fig. 4 with condensation rate 70%. Figure 12 represents $|\Psi_\nu(q)|^2$ ($\nu = 0, 1, 2$), numerically calculated from solving Eq. (31). The probability densities $|\Psi_\nu(q)|^2$ ($\nu = 0, 1, 2$) depend very little on \bar{r} , i.e., Ω . Furthermore we see that Fig. 12 resembles closely Fig. 5 for all the three cases with $\bar{r} = 3.8, 3.5$ and 3.2 fm. This means that the wavefunctions of the zero mode states depend little on the size of the condensate and condensation rate. This is parallel to the result that the excitation energies of the low-lying zero mode states are almost independent of the condensate size and the condensation rates. This is understood when we consider that the origin of the zero mode states is due to the SSB of the global phase of the condensate, which is independent of both the sizes and the condensation rates of the system.

3. Electric transition probabilities

Calculated $B(E2)$ and $M(E0)$ values are displayed in the column of Table II.

We note there that as the condensation rate increases from 70% to 100%, the E2 transition of $2_2^+ \rightarrow 0_2^+$ increases from 121 to 158, while the transition of $2_2^+ \rightarrow 0_3^+$ decreases from 76 to 62. Also the ratio $B(E2: 2_2^+ \rightarrow 0_2^+)/B(E2: 2_2^+ \rightarrow 0_3^+)$ changes from 1.59 to 2.5. With increasing condensation rate the transition of $2_2^+ \rightarrow 0_2^+$ is enhanced more than the $2_2^+ \rightarrow 0_3^+$ transition.

As for the monopole transitions, the strength of the monopole transition probabilities increases with increasing condensation rate, while the condensation rate does not affect the ratio $M(E0 : 0_2^+ \rightarrow 0_3^+)/M(E0 : 0_2^+ \rightarrow 0_3^+)$ much.

Thus, in our approach, the relative ratio of the E2 transitions and the strength of the E0 transitions sensitively reflects the condensation probabilities. The sensitivity of these quantities of the transitions may serve to the experimental determination of condensation rate of the Hoyle state. This sensitivity of the relative ratio of the E2 transitions is related to the vibrational nature of the BdG 2^+ state.

C. Energy levels of ^{12}C

In Fig. 13 the energy levels calculated with the parameters in Table I for each of $\bar{r} = 3.8, 3.5$ and 3.2 fm are shown in comparison with the experimental energy levels. The 0_4^+ state is identified as the second NG excited state $|\Psi_2\rangle|0\rangle_{\text{ex}}$, and its predicted energy level agrees well with the observed value for the whole calculated range of the \bar{r} . The small excitation energy of 0_3^+ state, less than 2 MeV, from the Hoyle, and the similar small energy between the 0_4^+ and 0_3^+ states are consistent with the picture that these two 0^+ states are due to the collective states of the NG operators. The almost same small excitation energy of the two 0^+ states despite of the change of the size of

the vacuum Hoyle state also supports that they are the zero mode states due to the SSB of the global phase of the vacuum. On the other hand, the calculated energy levels 2^+ and 4^+ of the lowest excitations of the BdG modes with $\ell = 2$ and $\ell = 4$ correspond to the observed 2_2^+ and 4_1^+ states, respectively. The agreement between the calculations and experiment is better for $\bar{r} = 3.8$ fm and is deteriorated for $\bar{r} = 3.5$ and 3.2 fm because the excitation energy increases with a larger Ω value in Table I in accordance with the vibrational nature of these states. Thus the observed 2_2^+ and 4_1^+ states are both interpreted as vibrational states on the BEC Hoyle state. The BdG energy levels in Fig. 13 show that the levels increase for smaller \bar{r} . The increase in Ω affects more dominantly on the levels than the decrease in V_r .

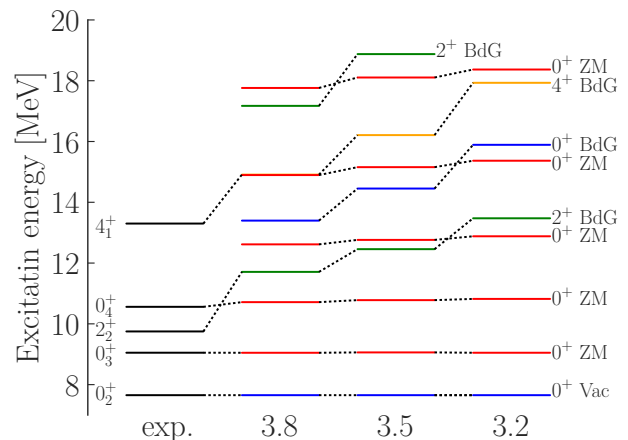


FIG. 13. (Color online) The energy levels of ^{12}C , calculated from the parameters in Table I with fixed $N_0 = 0.7N$ for $\bar{r} = 3.8, 3.5$ and 3.2 fm are compared with the experimental energy levels from Refs. [30, 31, 55–58]. Vac, ZM and BdG mean the vacuum Hoyle state, zero mode states and BdG excited states, respectively.

D. Robustness of the zero mode states for various condensation rates

We found that the energy levels in the realistic 70% condensation case barely change from those in the 100% condensation case. This means that in much small condensation rates such as 50%, 30% and 20%, the similar zero mode states could appear. Although the condensation rate in ^{12}C is reported to be as large as more than 60% in the theoretical cluster model calculations, it is intriguing to calculate the energy level structure under such hypothetical condensation rates, because in heavier mass region such as ^{52}Fe , in which we are interested from the viewpoint of universality of BEC of α cluster, the condensation rate could be much smaller than ^{12}C .

In Fig. 14 the energy levels calculated under condensation rates of 20%, 30% and 50% in comparison with those of 70% and 100% are displayed. We see that the

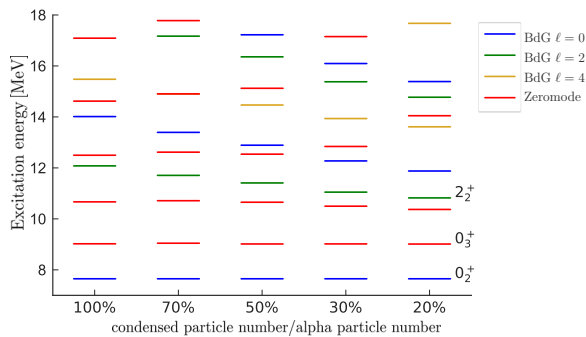


FIG. 14. (Color online) The energy levels of ^{12}C calculated with different condensation rates with $\bar{r} = 3.8$ fm.

structure of the energy levels of the first two low-lying zero mode states does not depend on the condensation rate, even for the smaller condensation rates. This is naturally understood because the zero mode states emerge once the global symmetry is spontaneously broken.

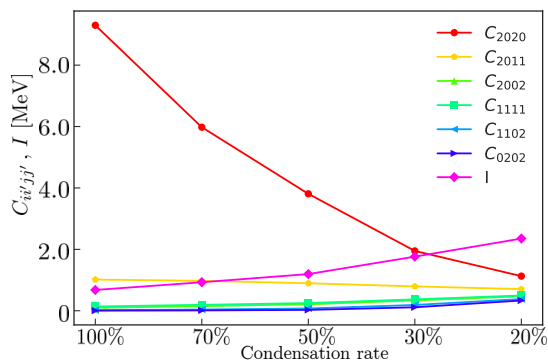


FIG. 15. (Color online) How the coefficient $C_{ijj'}$ of the zero mode Hamiltonian in Eq. (29) change in the calculations of Fig. 14 with different condensation rates of the three α clusters in ^{12}C is displayed.

As for the BdG modes the excitation energy decreases as the condensation rate decreases. However, the electric transitions to the BdG states are rather sensitive to the condensation rate of the three α clusters in ^{12}C . The transition probability changes, depending on the coefficient C_{2020} of the Q^4 term in Eq.(29). As seen in Fig.15, this term is overwhelmingly large than other terms.

It is worth noting that Bose-Einstein condensation of α clusters occurs even when the condensation rate is not 100%. In such a case α clusters that are not involved in condensation are sitting at the excited higher energy levels other than the lowest $0s$ state of the trapping potential. This partial involvement of α clusters in causing the Bose-Einstein condensation of α clusters reminds us the superfluidity of liquid HeII, in which the

observation of the momentum distribution by neutron inelastic scattering [63] showed that only about 13% of the atoms are in the lowest state at 1K and others are staying at the excited states. Also in the superfluid nuclei in heavy mass region where the pairing interaction is strong, Cooper pairs created only near the Fermi surface are responsible for causing superfluidity of nuclei. Many other nucleons are not needed to be paired as a Cooper pair. In fact, even several valence nucleons in the open shells outside the inert core in heavy nuclei cause superfluidity [2, 82, 83]. The present theoretical finding that Bose-Einstein condensation of α clusters is caused by partial condensation of α cluster as small as 20-30% in nuclei seems to be similar to Bose-Einstein condensation in other systems in nature. This is interesting and important, suggesting that α cluster condensation may be realized in a wide range of mass region in nuclei and also could be in nuclear matter and α cluster matter [64–66] at low densities.

VII. BOSE-EINSTEIN CONDENSATION OF MANY ALPHA CLUSTERS IN ^{16}O – ^{52}Fe

There is no reason that the BEC of α clusters is limited to the Hoyle and the related states of three α clusters, $N = 3$. It may occur for multi- α cluster systems with $N > 3$. Experimental and theoretical efforts have been devoted to search for such condensate states in heavier nuclei. Experimentally, however, it is not easy to detect multi- α clusters emitted with very low kinetic energies near the threshold in coincidence. Also it is not easy technically for the microscopic cluster models such as the RGM and GCM to solve the multi- α cluster problems up to $N = 13$ systematically. On the other hand, the present field theoretical superfluid α cluster model, in which the order parameter is embedded, has no difficulty in application to nuclei with a large number of α clusters like $N = 13$.

For ^{16}O with $N = 4$, experimentally much attention has been paid to four α cluster states with a linear chain structure for more than a decade since the observation by Chavallier *et al.* [67]. In Ref. [68] it was shown in the unified description of nuclear rainbows in $\alpha+^{12}\text{C}$ scattering and α cluster structures in the bound and quasi-bound low energy region of ^{16}O that the four α cluster states that have been considered to be a linear chain structure can be interpreted to have the $\alpha+^{12}\text{C}$ (0_2^+) structure in α cluster condensation. The observed 0^+ state at 15.1 MeV just above the four α threshold was suggested to be a Hoyle analogue four α condensate, similarly to the four α cluster model OCM calculations in Ref. [69]. As for the four α linear chain structure in ^{16}O , recent calculations suggest that their excitation energy is much higher than ever considered and as high as above 30 MeV [70, 71]. Itoh *et al.* [72] reported 386 MeV inelastic α scattering to search for a four α condensate in ^{16}O and observed two 0^+ states at 16.7 MeV with the $\alpha+^{12}\text{C}(0_2^+)$ structure and

18.8 MeV with the ${}^8\text{Be}+{}^8\text{Be}$ structure just above the four α threshold.

Beyond ${}^{16}\text{O}$ Freer *et al.* [73] searched for an α condensate state in ${}^{20}\text{Ne}$ by detecting five α clusters in the ${}^{12}\text{C}({}^{12}\text{C}, {}^8\text{Be}+{}^{12}\text{C}(0_2^+)){}^4\text{He}$ reactions and observed two ${}^{20}\text{Ne}$ resonances at 35.2 and 36.5 MeV. A theoretical study of four and five α condensates in ${}^{16}\text{O}$ and ${}^{20}\text{Ne}$, using a quasi-Schuck wave function, was made by Itagaki *et al.* [74]. Kawabata *et al.* [75] searched for six α condensates in ${}^{24}\text{Mg}$ in 400 MeV inelastic α scattering. Two α cluster condensation in ${}^{24}\text{Mg}$ and a three α cluster condensation in ${}^{28}\text{Si}$ were theoretically discussed using a quasi-Schuck wave function in Refs. [76, 77]. Akimune *et al.* [78] reported nine α clusters search in ${}^{36}\text{Ar}$. Also von Oertzen *et al.* [45–49] discussed the observed experimental signature of α condensation in ${}^{52}\text{Fe}$ and studied the three α cluster structure around the ${}^{40}\text{Ca}$ core. Akimune *et al.* [79] made inelastic α scattering from ${}^{56}\text{Ni}$ in inverse kinematic to observe α condensate state in ${}^{56}\text{Ni}$ and strongly suggested the existence of an α gas state at high excitation energies in ${}^{56}\text{Ni}$. Von Oertzen [80] discussed the conditions for a phase change with the formation of an α cluster condensate in excited compound nuclei up to ${}^{164}\text{Pb}$ based on the systematics for binding energies per α cluster in $N = Z$ nuclei. These investigations are encouraging and suggestive, however, no clear experimental evidence of BEC of α clusters such as α -cluster superfluidity or α cluster Josephson effect has been reported yet. It is therefore important and intriguing to explore, based on a firm theoretical frame of superfluid cluster model with order parameter, the BEC of α clusters systematically in heavier mass region beyond $N = 3$.

A. 100% condensation case

We calculate the energy levels of $N\alpha$ clusters of ${}^{16}\text{O}$ in the 0p-shell, ${}^{20}\text{Ne}$ – ${}^{40}\text{Ca}$ ($N = 4$ – 10) in the sd-shell of the light mass region, and ${}^{44}\text{Ti}$ – ${}^{52}\text{Fe}$ ($N = 11$ – 13) in the fp-shell of the medium-heavy mass region.

It is an unfounded claim that the parameters Ω and V_r are independent of N in our phenomenological model, but we have no general argument to determine their N -dependences. Here we presume that \bar{r} behaves as $N^{1/3}$, similarly as \bar{r} of the ordinary nuclei is proportional to $A^{1/3}$ with A being the mass number. Fixing $V_r = 400$ MeV, we adjust Ω for each N in such a manner that \bar{r} behaves as $N^{1/3}$. Figure 16 shows the N -dependence of Ω thus obtained, which is represented by the curve $\Omega = 5.4N^{-0.65}$.

In Fig. 17 the energy levels, given by calculations using this N -dependent Ω , are displayed. Figure 17 predicts the first zero mode state for each N below 2 MeV near the threshold energy, whose energy decreases as N becomes larger and which is expected to be observed in experiment. We note that for $N > 7$ the spectrum of the low-lying zero mode states becomes very similar. We therefore expect that similar zero mode states would ap-

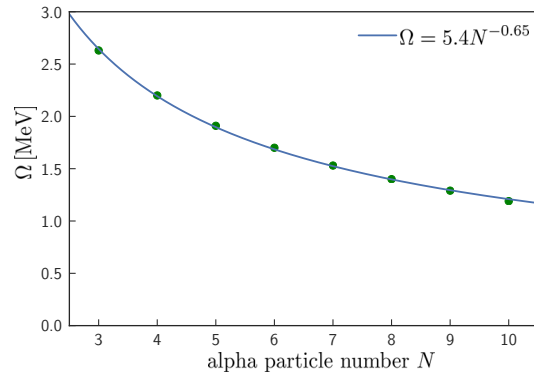


FIG. 16. The N -dependence of Ω of the confining potential, which is used in the energy level calculations of $N = 3$ – 13 (${}^{12}\text{C}$ – ${}^{52}\text{Fe}$) in Fig. 17, is displayed by the crosses. This is obtained under a constraint $\bar{r} \propto N^{1/3}$ and with fixed $V_r = 400$ MeV for 100% condensation. The solid curve $5.4N^{-0.65}$ is to guide the eye.

pear in heavier nucleus beyond ${}^{52}\text{Fe}$.

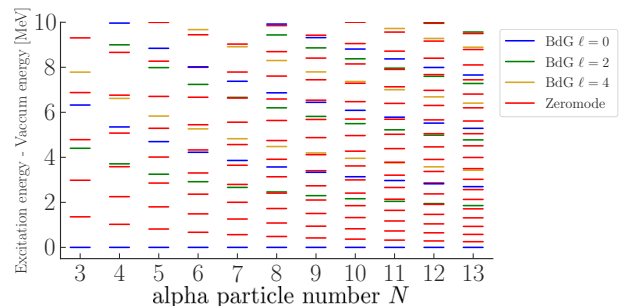


FIG. 17. (Color online) The energy levels calculated for $N = 3$ – 13 (${}^{12}\text{C}$ – ${}^{52}\text{Fe}$) with 100% condensation using N -dependent Ω given in Fig. 16. Excitation energy is measured from the Hoyle-analog vacuum, i.e., the N -alpha condensate state near the N -alpha threshold.

B. 70% condensation case

We have assumed 100% α cluster condensation $N_0 = N$ above, but in reality the condensation rate may not be necessarily 100% and may change from nucleus to nucleus. Similarly to ${}^{12}\text{C}$ in the previous sections, we here consider a case where $N\alpha$ clusters are condensed only partly, i.e., a typical case of $N_0 = 0.7N$.

We attempt to determine the parameter Ω for each N in such a manner that \bar{r} is proportional to $N^{1/3}$, setting $V_r = 400$ MeV and $N_0 = 0.7N$. The N -dependence of Ω is shown in Fig. 18, and is traced by the curve $\Omega = 4.70N^{-0.60}$. In Fig. 19 the energy levels calculated in the case of 70% condensation with the N -dependent Ω is

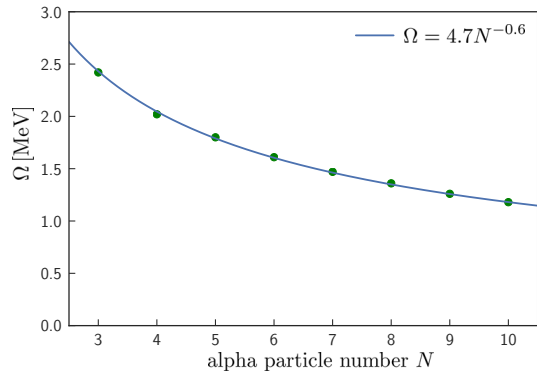


FIG. 18. The N -dependence of Ω of the confining potential in case of $N_0 = 0.7N$, which is used in the energy level calculations of $N = 3$ –13 (^{12}C – ^{52}Fe) in Fig. 19, is displayed by the crosses. This is obtained under a constraint $\bar{r} \propto N^{1/3}$ and with fixed $V_r = 400$ MeV. The solid curve $4.70N^{-0.60}$ is to guide the eye.

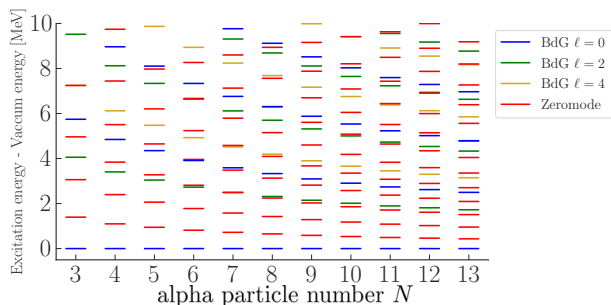


FIG. 19. (Color online) The energy levels calculated for $N = 3$ –13 (^{12}C – ^{52}Fe) in case of 70% condensation ($N_0 = 0.7N$) using the interaction with N -dependent Ω in Fig. 18. Excitation energy is measured from the Hoyle-analog vacuum, i.e., the N -alpha condensate state near the N -alpha threshold.

displayed. From Figs. 17 and 19, we see that the energy level structure is affected little by the condensation rate.

C. New soft mode of Bose–Einstein condensation of alpha clusters

The zero mode operator due to the BEC of α clusters emerge universally for any N , if α clusters are condensed only partly. Even under the condensation rate as small 20–30%, which may be likely in the actual nuclei, we have the zero mode, consisting of a series of zero mode states associated with the zero mode operators, in the same way as in the previous subsections. It is also noted that the first excited zero mode state appears less than 2 MeV above the threshold systematically for all the nuclei investigated here. The 0^+ states, identified as members states of the zero mode states, with low excitation energy

can be regarded as a soft mode. This is a new kind of soft mode due to the BEC of α clusters and has never been known in nuclei. The systematic appearance of this soft mode in a wide range of nuclei including light and heavy mass region is natural, since it originates from the locking of the global phase in gauge space that violates the number conservation.

The emergence of a soft mode in physical systems has been well-known [81]. The soft modes, by its definition [81], appear at low excitation energy from the ground state. In nuclei a soft mode of quadrupole collective motion appears in heavy nuclei under the quadrupole force. Then the NG zero mode connected to the spontaneous breaking of rotational symmetry plays a crucial role in the rotational motion [2]. Also pairing vibration and pairing rotation [82–84] are a soft mode in heavy superfluid nuclei in gauge space (number space) due to the spontaneous breaking of particle number symmetry caused by the pairing interaction, i.e. condensation of the Cooper pairs. The soft modes in hadronic systems have been studied extensively, see for example, see Ref.[85].

The vibrational and rotational collective motion due to α clustering, accompanied by SSB in Euclidean space, have been known. The vibrational motion is a radial (higher nodal) excitation of the relative motion and the rotational motion is due to the deformation caused by clustering. They have been observed in experiment, for example, typically as the $\mathcal{N} = 10$ higher nodal band and the parity doublet bands with the $\alpha+^{16}\text{O}$ cluster structure in ^{20}Ne [86], and the $\mathcal{N} = 14$ higher nodal band and the parity doublet bands with the $\alpha+^{40}\text{Ca}$ cluster structure in ^{44}Ti [10]. Here $\mathcal{N} = 2n + \ell$ with n and ℓ being the number of the nodes in the relative wave function between the clusters and the orbital angular momentum, respectively. However, no collective motion with soft mode nature related to α cluster condensation and SSB has been known so far. The collective states with low excitation energies as the zero mode states in the present study definitely possess soft mode nature. It is noted that the zero mode states emerge as 0^+ levels at very high excitation energies as well as at low excitation energy above the threshold.

The emergence of the well-developed 0_3^+ and 0_4^+ α cluster states in ^{12}C have been understood based on the geometrical configuration of α clusters in the traditional microscopic cluster models without an order parameter. For example, the 0_3^+ state has been interpreted to have an $\alpha+^8\text{Be}$ geometrical configuration with its relative motion being excited (higher nodal radial excitation) [87]. The 0_4^+ state has been interpreted to have a geometrical configuration of a linear chain [88, 89]. The origin of the emergence of the two 0_3^+ and 0_4^+ states just above the threshold has been ascribed to the specific structure of the 0_2^+ state (the Hoyle state) in ^{12}C . It is not clear if such two 0^+ states with low excitation energy also appear, for example, in ^{16}O with four alphas, ^{20}Ne with five alphas, ^{24}Mg with six alphas and ^{28}Si with seven alphas, *etc.*, before performing microscopic many α cluster

model calculations and/or *ab initio* calculations, which are formidably difficult nowadays for $N > 4$ or 5. Our viewpoint is that there may be a profound *raison d'être* for the very specific structure in ^{12}C that the collective three 0^+ states with a very developed dilute α cluster structure appear nearby within a couple of MeV just above the threshold. In other word, there may be an underlying fundamental principle related to symmetry that causes this specific structure in ^{12}C because emergence of a *collective motion with low excitation energy* is often related to an underlying symmetry of the system [81, 90–92]. In the present systematic calculations from $A = 12$ –52, it is found that the two 0^+ states appear just above the vacuum 0^+ state (analog of the Hoyle state) inevitably and universally as the zero mode states of the NG operators [90–92]. The present calculations have shown that even in the three α cluster system of ^{12}C , these gas-like 0_3^+ and 0_4^+ states can be understood as a collective motion that originates from the fundamental principle of SSB of the global phase. This is important because it enables us to expect the existence of such a gas-like α cluster states of BEC in the NG phase universally in light and heavy nuclei, which has never expected in the Ikeda diagram [93] in the configuration space considered in the Wigner phase. The emergence of the low-lying two 0^+ states above the Hoyle state is not accidental to ^{12}C but has a profound physical meaning of SSB of the global phase, which may persists as a emergence of a new kind of soft mode in light and heavy nuclei. It is interesting to search for experimentally not only the first two soft mode 0^+ states, which are observed in ^{12}C , but also higher members of low-lying soft mode states of the Nambu-Goldstone mode in light and heavy nuclei.

D. Characteristic of the zero mode spectrum

The spectrum of the zero mode states or collective states of the NG operators is derived from Eq. (31). There the Hamiltonian \hat{H}_u^{QP} in Eq. (29) is specified by the six coefficients $C_{ijj'j'}$ defined in Eq. (30) and the parameter I in Eq. (24). In the most naive estimation, which is valid for large N_0 and in which $\xi(r)$ and $\eta(r)$ behave as $\sqrt{N_0}$ and $1/\sqrt{N_0}$, respectively, the N -dependences are $C_{2020} \propto N_0^2$, $C_{2011} \propto N_0^1$, C_{2002} , $C_{1111} \propto N_0^0$, C_{1102} , $I \propto N_0^{-1}$, $C_{0202} \propto N_0^{-2}$, respectively. The results of actual numerical calculations for the coefficients $C_{ijj'j'}$ and I , ranging from $N_0 = 2$ to 13, are given in Fig. 21, indicating that the hierarchical order of the magnitudes is $C_{2020} > C_{2011} > I > C_{2002}$, $C_{1111} > C_{1102} > C_{0202}$ for the whole range of N_0 and that C_{1102} and C_{0202} are negligible.

The dominant contribution in \hat{H}_u^{QP} comes from the \hat{Q}^4 term with C_{2020} , and the \hat{P}^2 term can not be neglected due to the virial theorem. Thus the leading order zero mode Hamiltonian is the Hamiltonian for a one-dimensional quantum mechanical system under the \hat{Q}^4

potential,

$$\hat{H}_0^{QP} = \frac{I}{2}\hat{P}^2 + \frac{1}{2}C_{2020}\hat{Q}^4. \quad (53)$$

Figure 20 outlines the q^4 potential and the eigenfunctions $\Psi_\nu(q)$ belonging to the eigenvalues E_ν ($\nu = 0, 1, 2$) for \hat{H}_0^{QP} . The eigenvalues for \hat{H}_0^{QP} depends only on a single parameter of a dimension of energy $w = (I^2C_{2020})^{1/3}$. This is because \hat{H}_0^{QP} becomes

$$\hat{H}_0^{QP} = \frac{I'}{2}(\hat{P}')^2 + \frac{1}{2}C'_{2020}\hat{Q}'^4 \quad (54)$$

with $I' = s^2I$ and $C'_{2020} = C_{2020}/s^4$ when the scale transformation with a dimensionless parameter s , $\hat{Q}' = s\hat{Q}$ and $\hat{P}' = \hat{P}/s$, keeping $[\hat{Q}', \hat{P}'] = 1$, is performed. According to numerical calculations, the parameter w shows a very weak N_0 dependence as $N_0^{-0.08}$, and is almost constant. This implies that the spectrum of the zero mode states are almost the same regardless to a value of N_0 at this level of approximation, as in Fig. 22 (a).

The terms of the next orders in \hat{H}_u^{QP} are

$$\hat{H}_1^{QP} = 2C_{2011}\hat{Q}\hat{P}\hat{Q} - 2C_{2011}\hat{Q}^2, \quad (55)$$

$$\hat{H}_2^{QP} = -2(C_{2002} + C_{1111})\hat{P} + C_{2002}\hat{Q}\hat{P}^2\hat{Q}. \quad (56)$$

We see that \hat{H}_1^{QP} pushes down E_ν , while \hat{H}_2^{QP} pushes up E_ν , both larger for larger ν . The calculated spectrum of $\hat{H}_0^{QP} + \hat{H}_1^{QP} + \hat{H}_2^{QP}$ that approximates \hat{H}_u^{QP} well is plotted in Fig. 22 (b). It is seen there that the spectrum is almost independent of N_0 and that the corrections by $\hat{H}_1^{QP} + \hat{H}_2^{QP}$ shift the spectrum of \hat{H}_0^{QP} downwards for all the ν and N_0 .

We remark on the interpretations of \hat{Q} and \hat{P} , and the excitations in $\Psi_\nu(q)$. When the quantum fluctuation of \hat{Q} is small, it may be interpreted as the phase operator, as $(1 - i\hat{Q})\xi \simeq e^{-i\hat{Q}\xi}$, and the localization of $\Psi_0(q)$ around $q = 0$ corresponds to the phase locking. The excited wavefunctions $\Psi_\nu(q)$ ($\nu = 1, 2,$) are extended more widely as ν goes up, which implies that the excitation in the zero mode sector loosens the phase locking. However, the interpretation of \hat{Q} as the phase operator is valid only for small quantum fluctuations. As quantum fluctuations of \hat{Q} and \hat{P} become large due to a finite size of the system, the simple interpretation that \hat{Q} and \hat{P} are the phase operator and the generator of the phase transformation, respectively, breaks down. The operators \hat{Q} and \hat{P} should be treated as the canonical coordinate and momentum in a fictitious one-dimensional space, as is indicated by the field expansion in Eq. (26) and the commutation relation Eq. (27).

The analysis of this subsection serves as a general grasp of the energy levels of the 0^+ states, identified as the zero mode states, in Figs. 13, 6, 9, 14, 17 and 19.

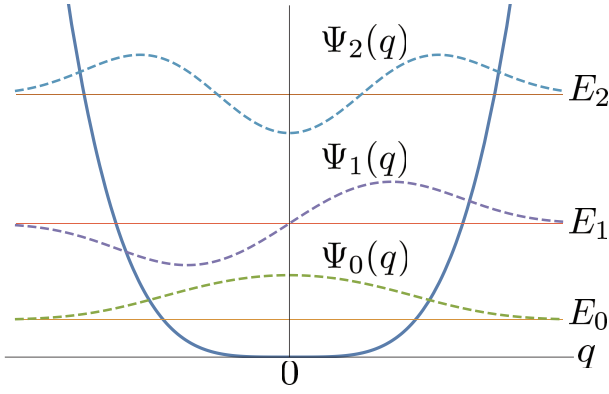


FIG. 20. (Color online) The q^4 potential and the eigenfunctions $\Psi_\nu(q)$ belonging to the eigenvalues E_ν ($\nu = 0, 1, 2$) for \hat{H}_0^{QP} .

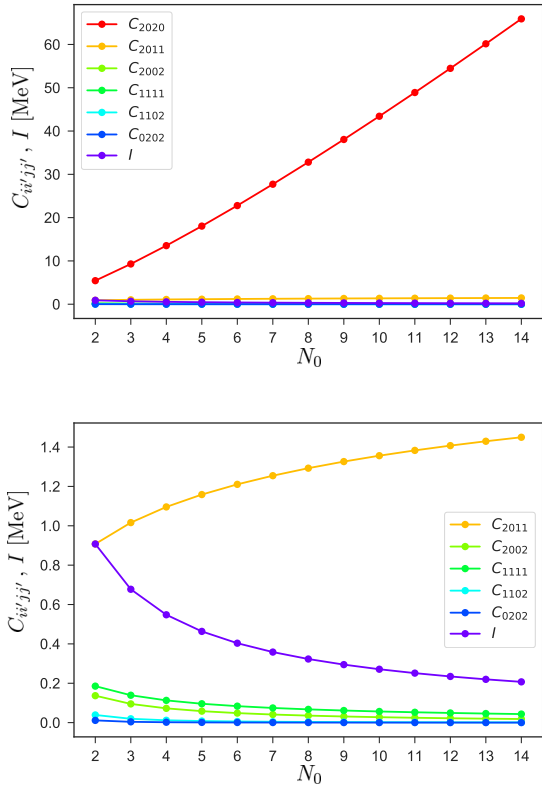


FIG. 21. (Color online) The N_0 -dependences of $C_{ijj'j'}$ and I with the parameters $V_r = 403[\text{MeV}]$, $\Omega = 2.62[\text{MeV}]$ and for $N_0 = 2-13$ are shown. (b) is a magnified graph of the small coefficients.

VIII. SUMMARY

Bose–Einstein condensation (BEC) of α clusters in light and medium-heavy $4N$ nuclei is studied in the frame of the field theoretical superfluid cluster model.

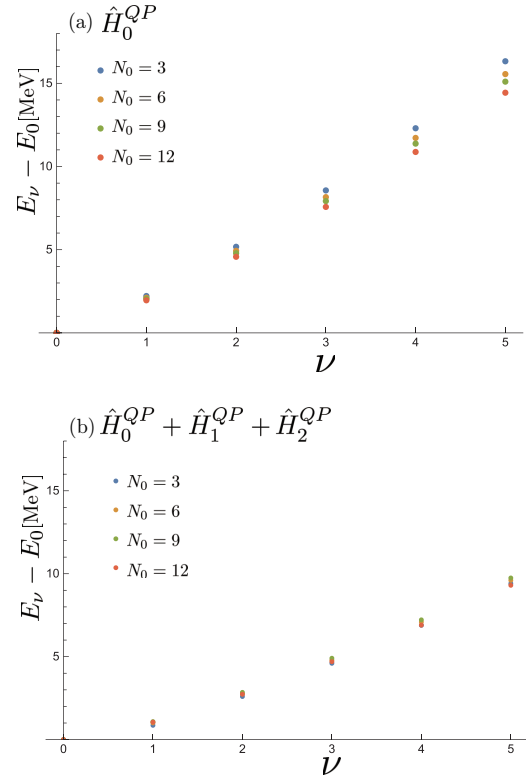


FIG. 22. (Color online) Numerically calculated excitation energies $E_\nu - E_0$ of (a) \hat{H}_0^{QP} and (b) $\hat{H}_0^{QP} + \hat{H}_1^{QP} + \hat{H}_2^{QP}$ are plotted for $\nu = 1-5$ and $N_0 = 3, 6, 9, 12$ with the parameters $V_r = 403[\text{MeV}]$ and $\Omega = 2.62[\text{MeV}]$.

There it is crucial that the order parameter is expressed as the vacuum expectation of the field operator explicitly. The order parameter is a superfluid amplitude that satisfies Gross–Pitaevskii equation and characterizes the phase transition from the normal α cluster state in the Wigner phase to the Nambu–Goldstone phase with Bose–Einstein condensate of α clusters. The Nambu–Goldstone operators (zero mode operators) due to spontaneous symmetry breaking of the global phase in the *finite* number of α clusters is rigorously treated. We have analyzed the α cluster structure in ^{12}C , assuming a realistic condensation rate. It is found that the energy levels of the α cluster structure above the Hoyle state are well reproduced. The well-developed 2^+ and 4^+ states are understood to be Bogoliubov–de Gennes vibrational modes built on the Hoyle state rather than a rotational band. The calculations at various condensation rates have revealed that the similar energy level structures are appear repeatedly once the BEC is realized, even if the condensation rate is not very large.

It is found in the superfluid cluster model with the order parameter that the two gas-like collective 0_3^+ and 0_4^+ states above the Hoyle state in ^{12}C , which have been understood in the traditional cluster models based on a geometrical configuration space, can be understood as a

manifestation of the emergence of the zero mode that has a profound field theoretical physical meaning of the locking of the global phase in the gauge space. The present theory of ^{12}C was extended to $N\alpha$ nuclei, ^{16}O – ^{52}Fe , in light and medium-heavy mass region, assuming different condensation rates of α clusters. Then, due to spontaneous symmetry breaking, we similarly have the zero mode operators and the associated zero mode states in these nuclei, even if the condensation rates are not very large. The energy level structure of the zero mode 0^+ states change little, depending on the N and the condensation rates. This means that the collective 0^+ states with low excitation energy appear systematically above the threshold energy in light and heavy nuclei. They are new kind of soft mode states due to the BEC of α clusters. It is highly expected to search for such a soft mode in experiment. The field theoretical superfluid cluster model may be applicable to much heavier nuclei beyond the present study. It is expected that the new zero mode states, originating from the spontaneous sym-

metry breaking of the global phase of the superfluid α clusters in nuclei may persist throughout the periodic table from light nuclei to heavy nuclei. The application of the present field theoretical superfluid cluster model study to the heavy mass region around ^{212}Po is a future challenging subject.

ACKNOWLEDGMENTS

This work is supported by JSPS KAKENHI Grant No. 16K05488. The authors thank Yasuhiro Nagai and Ryo Yoshioka for their numerical calculations at an early stage of this work, and the Yukawa Institute for Theoretical Physics, Kyoto University for making possible the present collaborative work. One of the authors (SO) is also grateful to the Research Center for Nuclear Physics, Osaka University for supporting the present work. Part of this work was done during the authors' stay in YITP in 2018.

-
- [1] A. Bohr and B. R. Mottelson: *Nuclear Structure*, Vol. II, (Benjamin, Inc., New York).
- [2] P. Ring and P. Schuck, *The nuclear many-body problem* (Springer-Verlag, Berlin, 1980).
- [3] K. Ikeda, T. Marumori, R. Tamagaki, and H. Tanaka, Prog. Theor. Phys. Suppl. **52**, 1 (1972) and references therein.
- [4] K. Ikeda, H. Horiuchi, and S. Saito, Prog. Theor. Phys. Suppl. **68**, 1 (1980) and references therein.
- [5] S. Ohkubo, M. Fujiwara, and P. E. Hodgson, Prog. Theor. Phys. Suppl. **132**, 1 (1998); S. Ohkubo, T. Yamaya, and P. E. Hodgson, Nuclear clusters, in *Nucleon-Hadron Many-Body Systems*, (edited by H. Ejiri and H. Toki) (Oxford University Press, Oxford, 1999), p. 150 and references therein.
- [6] K. Wildermuth and Y. C. Tang, *A Unified Theory of the Nucleus* (Vieweg, Braunschweig, 1977).
- [7] M. G. Mayer, Phys. Rev. **75**, 1969 (1949).
- [8] O. Haxel, J. H. D. Jensen, and H. E. Suess, Phys. Rev. **75**, 1766 (1949).
- [9] A. Bohr, Dan. Mat. Fys. Medd. **26**, No.14 (1952); A. Bohr and B. R. Mottelson, Dan. Mat. Fys. Medd. **27**, No.16 (1953).
- [10] F. Michel, S. Ohkubo, and G. Reidemeister, Prog. Theor. Phys. Suppl. **132**, 7 (1998).
- [11] T. Yamaya, K. Katori, M. Fujiwara, S. Kato, and S. Ohkubo, Prog. Theor. Phys. Suppl. **132**, 73 (1998).
- [12] T. Sakuda and S. Ohkubo, Prog. Theor. Phys. Suppl. **132**, 103 (1998).
- [13] B. Buck, A. C. Merchant, and S. M. Perez, Phys. Rev. Lett. **72**, 1326 (1994).
- [14] S. Ohkubo, Phys. Rev. Lett. **74**, 2176 (1995).
- [15] A. Astier, P. Petkov, M.-G. Porquet, D. S. Delion, and P. Schuck, Phys. Rev. Lett. **104**, 042701 (2010).
- [16] Y. Suzuki and S. Ohkubo, Phys. Rev. C **82**, 041303 (R) (2010).
- [17] J. Eichler and M. Yamamura, Nucl. Phys. **A 182**, 33 (1972).
- [18] Y. K. Gambhir, P. Ring, and P. Schuck, Phys. Rev. Lett. **51**, 1253 (1983).
- [19] S. Koh, Prog. Theor. Phys. Suppl. **132**, 197 (1998).
- [20] Y. Fujiwara and R. Tamagaki, Prog. Theor. Phys. **59**, 1503 (1976).
- [21] E. Uegaki, S. Okabe, Y. Abe, and H. Tanaka, Prog. Theor. Phys. **57**, 1262 (1977); E. Uegaki, Y. Abe, S. Okabe, and H. Tanaka, Prog. Theor. Phys. **62**, 1621 (1979).
- [22] Y. Fukushima and M. Kamimura, J. Phys. Soc. Jpn. **44**, 225 (1978); M. Kamimura, Nucl. Phys. **A 351**, 456 (1981).
- [23] A. Tohsaki, H. Horiuchi, P. Schuck, and G. Röpke, Phys. Rev. Lett. **87**, 192501 (2001).
- [24] Y. Funaki, Phys. Rev. C **92**, 021302 (R) (2015).
- [25] H. Matsumura and Y. Suzuki, Nucl. Phys. **A 739**, 238 (2004).
- [26] C. Kurokawa and K. Kato, Nucl. Phys. **A 738**, 455 (2004).
- [27] S. Ohtsubo, Y. Fukushima, M. Kamimura, and E. Hiyama, Prog. Theor. Exp. Phys., 073D02 (2013) and earlier references therein.
- [28] B. Buck, A. C. Merchant, and S. M. Perez, Phys. Rev. C **45**, 1688 (1992).
- [29] Y. Nakamura, J. Takahashi, Y. Yamanaka, and S. Ohkubo, Phys. Rev. C **94**, 014314 (2016) and earlier references therein.
- [30] M. Freer *et al.*, Phys. Rev. C **83**, 034314 (2011) and earlier references therein.
- [31] M. Itoh *et al.*, Nucl. Phys. **A 738**, 268 (2004); M. Itoh *et al.*, Phys. Rev. C **84**, 054308 (2011).
- [32] O. Kirsebom, Physics **10**, 103 (2017).
- [33] D. Dell'Aquila *et al.*, Phys. Rev. Lett. **119**, 132501 (2017).
- [34] R. Smith, Tz. Kokalova, C. Wheldon, J. E. Bishop, M. Freer, N. Curtis, and D. J. Parker, Phys. Rev. Lett. **119**,

- 132502 (2017).
- [35] Y. Kanada-En'yo, Prog. Theor. Phys. **117**, 655 (2007).
- [36] M. Chernykh, H. Feldmeier, T. Neff, P. von Neumann-Cosel, and A. Richter, Phys. Rev. Lett. **98**, 032501 (2007).
- [37] R. Roth, J. Langhammer, A. Calci, S. Binder, and P. Navratil, Phys. Rev. Lett. **107**, 072501 (2011).
- [38] E. Epelbaum, H. Krebs, T. A. Lähde, D. Lee, and U.-G. Meißner, Phys. Rev. Lett. **106**, 192501 (2011).
- [39] T. Sakuda and S. Ohkubo, Nucl. Phys. **A 744**, 77 (2004); Nucl. Phys. **A 748**, 699 (2005).
- [40] T. Sakuda and S. Ohkubo, Nucl. Phys. **A 908**, 73 (2013).
- [41] P. Descouvemont, Nucl. Phys. **A 709**, 275 (2002).
- [42] T. Sakuda and S. Ohkubo, Nucl. Phys. **A 712**, 59 (2002).
- [43] P. Mohr, Eur. Phys. J. **A53**, 209 (2017).
- [44] T. Yamada and P. Schuck, Phys. Rev. C **69**, 024309 (2004).
- [45] Tz. Kokalova, N. Itagaki, W. von Oertzen, and C. Wheldon, Phys. Rev. Lett. **96**, 192502 (2006).
- [46] N. Itagaki, Tz. Kokalova, and W. von Oertzen, Phys. Rev. C **82**, 014312 (2010).
- [47] W. von Oertzen, J. Phys. Conf. Ser. **321**, 012035 (2011).
- [48] N. Itagaki, Tz. Kokalova, W. von Oertzen, and J. A. Maruhn, Int. J. Mod. Phys. E **20**, 1012 (2011).
- [49] Tz. Kokalova *et al.*, Eur. Phys. J. A **23**, 19 (2003).
- [50] S. Ali and A. R. Bodmer, Nucl. Phys. **A 80**, 99 (1966).
- [51] E. P. Gross, Nuovo Cimento **20**, 454 (1961); J. Math. Phys. **4**, 195 (1963); L. P. Pitaevskii, Zh. Eksp. Teor. Fiz. **40**, 646 (1961).
- [52] H. Umezawa, H. Matsumoto, and M. Tachiki, *Thermo Field Dynamics and Condensed States* (North-Holland, Amsterdam, 1982).
- [53] Y. Nakamura, J. Takahashi, and Y. Yamanaka, Phys. Rev. A **89**, 013613 (2014).
- [54] T. Yamada and P. Schuck, Eur. Phys. J. **A 26**, 185 (2005).
- [55] M. Freer *et al.*, Phys. Rev. C **80**, 041303 (R) (2009).
- [56] W. R. Zimmerman, N. E. Destefano, M. Freer, M. Gai, and F. D. Smit, Phys. Rev. C **84**, 027304 (2011).
- [57] W. R. Zimmerman *et al.*, Phys. Rev. Lett. **110**, 152502 (2013).
- [58] M. Itoh *et al.*, J. Phys. Conf. Ser. **436**, 012006 (2013).
- [59] B. D. Josephson, Phys. Lett. **21**, 608 (1966).
- [60] D. M. Ceperley, Rev Mod. Phys. **67**, 279 (1995); D. M. Ceperley and E. Manousakis, J. Chem. Phys. **115**, 10111 (2001).
- [61] B. C. Mulkerin, L. He, P. Dyke, C. J. Vale, X. J. Liu, and H. Hu, Phys. Rev. A **96**, 053608 (2017).
- [62] K. Kobayashi, Y. Nakamura, M. Mine, and Y. Yamanaka, Ann. Phys. **324**, 2359 (2009).
- [63] V. F. Sears, E. C. Svensson, P. Martel, and A. D. B. Woods Phys. Rev. Lett. **49**, 279 (1982) and references therein.
- [64] J. W. Clark and T. P. Wang, Ann. Phys. (NY) **40**, 127 (1966).
- [65] A. Tohsaki, Prog. Theor. Phys. Suppl. **132**, 213 (1998).
- [66] F. Carstoiu and S. Misicu, Phys. Lett. **B 682**, 33 (2009).
- [67] P. Chevallier, F. Scheibling, G. Goldring, I. Plesser, and M. W. Sachs, Phys. Rev. **160**, 827 (1967).
- [68] S. Ohkubo and Y. Hirabayashi, Phys. Lett. **B 684**, 127 (2010).
- [69] Y. Funaki, T. Yamada, H. Horiuchi, G. Röpke, P. Schuck, and A. Tohsaki, Phys. Rev. Lett. **101**, 082502 (2008).
- [70] T. Ichikawa, J. A. Maruhn, N. Itagaki, and S. Ohkubo Phys. Rev. Lett. **107**, 112501 (2011) and references therein.
- [71] W. Horiuchi and Y. Suzuki, Phys. Rev. C **95**, 044320 (2017).
- [72] M. Itoh *et al.*, J. Phys. Conf. Ser. **569**, 012009 (2014).
- [73] M. Freer *et al.*, Phys. Rev. C **71**, 047305 (2005).
- [74] N. Itagaki, Tz. Kokalova, M. Ito, M. Kimura, and W. von Oertzen, Phys. Rev. C **78**, 037301 (2008).
- [75] T. Kawabata *et al.*, J. Phys. Conf. Ser. **436**, 012009 (2013).
- [76] N. Itagaki, M. Kimura, C. Kurokawa, M. Ito, and W. von Oertzen Phys. Rev. C **75**, 03730 (2007).
- [77] T. Ichikawa, N. Itagaki, Y. Kanada-Enyo, Tz. Kokalova, and W. von Oertzen, Phys. Rev. C **86**, 031303 (R) (2012).
- [78] H. Akimune *et al.*, 4th Joint Meeting of the APS Division of Nucl. Phys. and the Phys. Soc. of Japan, **59**, Number 10 (Oct. 7-11, 2014; Waikoloa, Hawaii), abstract id. EF.004.
- [79] H. Akimune *et al.*, J. Phys. Conf. Ser. **436**, 012010 (2013).
- [80] W. von Oertzen, Eur. Phys. J. A **29**, 133 (2006).
- [81] P. W. Anderson, *Basic Notions of Condensed Matter Physics* (Benjamin, London, 1984).
- [82] R. A. Broglia, O. Hansen, and C. Riedel, Adv. Nucl. Phys. **6**, 259 (1973); R. A. Broglia, J. Terasaki, and N. Giovanardi, Phys. Rep. **335**, 1 (2000).
- [83] D. M. Brink and R. A. Broglia, *Nuclear Superfluidity: Pairing in Finite Systems* (Cambridge University Press, Cambridge, 2005).
- [84] N. Hinohara and W. Nazarewicz, Phys. Rev. Lett. **116**, 152502 (2016).
- [85] T. Hatsuda and T. Kunihiro, Phys. Rep. **247**, 221 (1994).
- [86] Y. Fujiwara *et al.*, Prog. Theor. Phys. Suppl. **68**, 29 (1980).
- [87] C. Kurokawa and K. Katō, Nucl. Phys. **A 792**, 87 (2007).
- [88] T. Suhara, Y. Funaki, B. Zhou, H. Horiuchi, and A. Tohsaki, Phys. Rev. Lett. **112**, 062501 (2014).
- [89] Y. Funaki, Phys. Rev. C **94**, 024344 (2014).
- [90] Y. Nambu and G. Jona-Lasinio, Phys. Rev. **122**, 345 (1961).
- [91] H. Watanabe and H. Murayama, Phys. Rev. Lett. **108**, 251602 (2012).
- [92] Y. Hidaka, Phys. Rev. Lett. **110**, 091601 (2013).
- [93] K. Ikeda, N. Takigawa, and H. Horiuchi, Prog. Theor. Phys. Suppl. **E68**, 464 (1968).